ELSEVIER

Comput. Methods Appl. Mech. Engrg. 125 (1995) 187–220

Computer methods in applied mechanics and engineering

Numerical solution of two-carrier hydrodynamic semiconductor device equations employing a stabilized finite element method

N.R. Aluru, K.H. Law*, A. Raefsky, P.M. Pinsky, R.W. Dutton

Integrated Circuits Laboratory, 231-F, Applied Electronics Laboratory, Stanford University, Stanford, CA 94309, USA

Received 12 July 1994

Abstract

A space–time Galerkin/least-squares finite element method was presented in [1] for numerical simulation of single-carrier hydrodynamic semiconductor device equations. The single-carrier hydrodynamic device equations were shown to resemble the ideal gas equations and Galerkin/least-squares finite element method, originally developed for computational fluid dynamics equations [16], was extended to solve semiconductor device applications. In this paper, the space–time Galerkin/least-squares finite element method is further extended and generalized to solve two-carrier hydrodynamic device equations. The proposed formulation is based on a time-discontinuous Galerkin method, in which physical entropy variables are employed. A standard Galerkin finite element method is applied to the Poisson equation. Numerical simulations are performed on the coupled Poisson and the two-carrier hydrodynamic equations employing a staggered approach.

A mathematical analysis of the time-dependent multi-dimensional hydrodynamic model is performed to determine well-posed boundary conditions for electrical contacts. The number of boundary conditions that need to be specified for the hydrodynamic equations at inflow and outflow boundaries of the device are derived. Example boundary conditions that are based either on physical and/or mathematical basis are presented.

Stability of the numerical algorithms is addressed. The space–time Galerkin/least-squares finite element method and the standard Galerkin finite element method for the hydrodynamic and Poisson equations, respectively, are shown to be stable. Specifically, a Clausius–Duhem inequality, a basic stability requirement, is derived for the hydrodynamic equations and the proposed numerical method automatically satisfies this stability requirement. Numerical simulations are performed on one- and two-dimensional two-carrier p-n diodes and the results demonstrate the effectiveness of the proposed numerical method.

Notation

α	particle identification; takes the value of 1 for electrons or 2 for holes
Γ	boundary of spatial domain
Γ_g	spatial boundary where essential boundary conditions are prescribed
Γ_h	spatial boundary where natural boundary conditions are prescribed
$\mathscr{H}_\alpha$	generalized entropy function for the αth particle
θ	dielectric permittivity
κ_α	heat-conductivity of the αth particle
$\mathscr{L}_\alpha$	differential operator for the αth particle
$\lambda_{\alpha ij}$	eigenvalues of convective Jacobian matrix for the αth particle
$\mu_{0\alpha}$	low-field mobility of the αth particle
μ_α	specific chemical potential of the αth particle
Ω	spatial domain

* Corresponding author.

SSDI 0045-7825(94)00794-2

Ω_n^e element spatial domain at the nth time slab
ψ electrostatic potential
$\bar{\psi}$ weighting function for the Poisson equation
ψ_{appl} applied bias
ψ_b built-in potential
$\tau_{\text{GLS}\alpha}$ intrinsic time scales matrix of the αth particle employed in Galerkin/least-squares formulation
τ_1 electron life time
τ_2 hole life time
$\tau_{p\alpha}$ momentum relaxation time for the αth particle
$\tau_{w\alpha}$ energy relaxation time for the αth particle
γ_α constant defining ratio of specific heats for the αth particle
δ_{ij} Kronecker delta; $=1$ for $i=j$ and 0 otherwise
$[\ ]_{\text{col}}$ collision terms
$\boldsymbol{A}_{\alpha i}$ convective Jacobian matrix of the αth particle with respect to conservation variables in direction i
$\tilde{\boldsymbol{A}}_{\alpha 0}$ Riemannian metric tensor for the αth particle
$\tilde{\boldsymbol{A}}_{\alpha i}$ convective Jacobian matrix of the αth particle with respect to entropy variables in direction i
$\hat{\boldsymbol{A}}_{\alpha i}$ convective Jacobian matrix of the αth particle with respective primitive variables in direction i
B_n boundary of nth space time slab
$\boldsymbol{B}(.,.)_{\alpha n}$ left-hand side operator for the weak form of the hydrodynamic equations for the αth particle at time level n
$\boldsymbol{B}_{\text{GAL}}(.,.)_{\alpha n}$ left-hand side operator for the Galerkin form of the hydrodynamic equations for the αth particle at time level n
$\boldsymbol{B}_{\text{GLS}}(.,.)_{\alpha n}$ left-hand side operator for the Galerkin/least-squares form of the hydrodynamic equations for the αth particle at time level n
$B_p(.,.)$ left-hand side operator for the Poisson equation
C_α speed of sound for the αth particle
$\boldsymbol{D}_\alpha$ vector of non-linear boundary conditions for the αth particle
$\boldsymbol{E}$ electric field vector
E_i electric field along direction i
$\boldsymbol{F}_\alpha$ source vector for the αth particle
$\hat{\boldsymbol{F}}_\alpha$ source vector for the αth particle when primitive variables are used
$\boldsymbol{F}_{\alpha i}^{\text{c}}$ convective flux vector for the αth particle in direction i
$\boldsymbol{F}_{\alpha i}^{\text{h}}$ heat flux vector for the αth particle in direction i
G avalanche generation term (neglected in this paper)
I_n nth time interval
$\boldsymbol{K}_{\alpha ij}$ diffusion matrix for the αth particle with respect to conservation variables in directions i, j
$\tilde{\boldsymbol{K}}_{\alpha ij}$ diffusion matrix for the αth particle with respect to entropy variables in directions i, j
$\hat{\boldsymbol{K}}_{\alpha ij}$ diffusion matrix for the αth particle with respect to primitive variables in directions i, j
$\boldsymbol{L}(.)_{\alpha n}$ right-hand side operator for the weak form of the hydrodynamic equations for the αth particle at time level n
$\boldsymbol{L}_{\text{GAL}}(.)_{\alpha n}$ right-hand side operator for the Galerkin form of the hydrodynamic equations for the αth particle at time level n
$\boldsymbol{L}_{\text{GLS}}(.)_{\alpha n}$ right-hand side operator for the Galerkin/least-squares form of the hydrodynamic equations for the αth particle at time level n
$L_p(.)$ right-hand side operator for the Poisson equation
$N_A^{(n)}$ finite element spatial shape function of node A for the nth time slab
N_{A}^- concentration of ionized acceptor

N_D^+	concentration of ionized donor
P_α	pressure of the αth particle
Q_n	space time slab at time level n
Q_n^e	element space time slab at time level n
R_α	gas constant of the αth particle
R, R_{SRH}, R_{AU}	recombination, Shockley–Read–Hall recombination and Auger recombination
T_0	lattice temperature
T_α	temperature of the αth particle
U_α	conservative variable vector of the αth particle
$\hat{U}_\alpha$	primitive variable vector of the αth particle
V_α	entropy variable vector of the αth particle
c_α	carrier concentration of the αth particle
c_1	concentration of electrons
c_2	concentration of holes
c_{int}	intrinsic carrier concentration
$c_{v\alpha}$	specific heat of the αth particle at constant volume
e_α^{int}	internal energy of the αth particle per unit mass
e_α^{kin}	kinetic energy of the αth particle per unit mass
e_α^{tot}	total energy of the αth particle per unit mass
$g_{\alpha i}$	prescribed boundary conditions of the αth particle along direction i
k_b	Boltzmann constant
m_0	free electron mass
m_α	mass of the αth particle
m_1	electron mass
m_2	hole mass
n_i	unit outward normal
n_{dof}	number of degrees of freedom for hydrodynamic equations
$(n_{el})_n$	number of space–time finite elements at time level n
n_{sd}	number of space dimensions
p_α	momentum density vector of the αth particle
q_α	heat flux vector of the αth particle
$q_{\alpha i}$	heat flux of the αth particle along direction i
s_α	thermodynamic entropy of the αth particle per unit mass
u_α	velocity vector of the αth particle
$u_{\alpha i}$	velocity of the αth particle along direction i
$v_{s\alpha}$	saturation velocity of the αth particle
$v_{\alpha A}^{(n+1)}$	vector of nodal unknowns at node A for the hydrodynamic system of the αth particle at time level $n+1$
w_α	energy density of the αth particle
$w_{\alpha A}^{(n+1)}$	vector of weighting functions at node A for the hydrodynamic system of the αth particle at time level $n+1$
$w_{0\alpha}$	equilibrium energy density of the αth particle
X'	denotes the variation of X
$(\,)^h$	denotes a finite element approximation
$(\,)_0$	denotes a reference value

1. Introduction

The classical drift-diffusion (DD) equations for semiconductor device modeling assume a simple linear relationship between carrier velocity and the local electric field and negligible temperature gradients. The first assumption suppresses the velocity overshoot phenomena where the velocity can

locally exceed the asymptotic limit placed by the DD model and the second assumption suppresses the carrier heating phenomena. With the scaling of silicon devices into deep submicron regimes, non-stationary phenomena such as velocity overshoot and carrier heating are becoming increasingly important to determine the characteristics of these devices. As a result, there has been a shift away from the commonly employed DD model and advanced transport models, such as the energy transport (ET) and the hydrodynamic (HD) models, have become increasingly popular. Both energy transport and hydrodynamic models can be derived from the Boltzmann Transport Equation (BTE) and the hydrodynamic model involves fewer assumptions compared to the energy transport model. In the hydrodynamic model, the carrier drift velocity is solved explicitly and this is needed for accurate description of the state-of-the-art devices. Hence, the selection of the hydrodynamic model for semiconductor device simulation in this study.

The electrical current inside a material results from the transport of mobile charges called carriers. For semiconductors, after applying the energy band model to the periodic potentials of the crystal lattice, these carriers can be viewed as two types of oppositely-charged free articles moving in vacuum with modified effective mass and permittivity. The positively-charged carriers are called holes and the negatively-charged carriers are called electrons. Comprehensive semiconductor device simulation based on the hydrodynamic model involves solving a system of coupled electron hydrodynamic equations, hole hydrodynamic equations and the Poisson equation. This system is referred to as a two-carrier (involving both electrons and holes) hydrodynamic transport model. The device operation can be approximated by single-carrier (either electron or hole) in some simplified cases and numerical results based on the hydrodynamic model have been presented for single-carrier devices [1, 2, 8, 9, 24]. In [8, 9, 24] finite difference and volume based schemes were employed. In our work [1, 2], a space–time Galerkin/least-squares (GLS) finite element scheme was employed. Finite element methods provide a more general framework than finite difference or volume based schemes, but are generally considered unsuitable for device applications [25]. The complex interaction between electrons and holes gives rise to solutions which vary several orders of magnitude within a few Angstroms. Robust numerical schemes are needed to guarantee stability, convergence and accuracy. In this paper the finite element numerical scheme presented in [1] is generalized to solve two-carrier hydrodynamic device equations. Our numerical results dispel the myth that finite elements are not suitable for semiconductor device simulation.

This paper addresses a number of numerical and mathematical issues related to the hydrodynamic model. First, the resemblance of the hydrodynamic equations to the ideal gas equations is exploited. The finite element numerical schemes developed by Hughes et al. [16] for compressible Euler and Navier–Stokes equations are extended to efficiently solve the coupled hydrodynamic equations. Second, the issue of boundary conditions for the hydrodynamic model is addressed. The number of boundary conditions to be specified for electrical contacts are derived and it is shown that the number of boundary conditions to be specified for the hydrodynamic model are different from those of the Euler and Navier–Stokes equations. Several sets of boundary conditions are proposed for subsonic/supersonic inflows/outflows. Practical difficulties in specifying well-posed conditions are addressed. Third, the stability of the proposed numerical schemes is established. Specifically, Clausius–Duhem inequalities are derived for the hydrodynamic device equations and the numerical scheme is shown to satisfy these inequalities.

This paper is organized as follows: Section 2 introduces the two-carrier hydrodynamic semiconductor device equations and the Poisson equation. Section 3 describes the assumptions employed in the hydrodynamic model, discusses the relationship to ideal gas equations, presents a conservation form on which the symmetrization procedures are developed, and introduces a finite element variational formulation. Section 4 presents theoretical results on boundary conditions. Section 5 discusses the GLS numerical scheme for hydrodynamic equations, establishes the stability and consistency of the numerical scheme. Section 6 presents a brief overview of the standard Galerkin finite element method for Poisson equations and establishes the stability and consistency of the method. Section 7 presents the solution scheme to solve the coupled two-carrier hydrodynamic and Poisson equations. Section 8 presents numerical results for one-dimensional and two-dimensional diodes and conclusions are presented in Section 9.

2. Semiconductor equations

The motion of electrons and holes within a semiconductor can be best described by the integro-differential Boltzmann Transport Equation. Closed-form solution for this equation is not possible except for a few simple cases. The most successful approach to solve the BTE is by Monte Carlo simulation. An attractive alternative for semiconductor device simulation is to employ the hydrodynamic model. The hydrodynamic semiconductor device equations can be derived from the BTE by considering the first three moments, defining, respectively, the particle continuity, conservation of momentum and energy [5] for the electrons and holes. The two systems of equations obtained from the first three moments of BTE can be summarized as follows

$$\frac{\partial c_\alpha}{\partial t} + \nabla \cdot (c_\alpha \boldsymbol{u}_\alpha) = \left[\frac{\partial c_\alpha}{\partial t}\right]_{\text{col}} \tag{1}$$

$$\frac{\partial \boldsymbol{p}_\alpha}{\partial t} + \boldsymbol{u}_\alpha(\nabla \cdot \boldsymbol{p}_\alpha) + (\boldsymbol{p}_\alpha \cdot \nabla)\boldsymbol{u}_\alpha = (-1)^\alpha \varepsilon c_\alpha \boldsymbol{E} - \nabla(c_\alpha k_b T_\alpha) + \left[\frac{\partial \boldsymbol{p}_\alpha}{\partial t}\right]_{\text{col}} \tag{2}$$

$$\frac{\partial w_\alpha}{\partial t} + \nabla \cdot (\boldsymbol{u}_\alpha w_\alpha) = (-1)^\alpha \varepsilon c_\alpha (\boldsymbol{u}_\alpha \cdot \boldsymbol{E}) - \nabla \cdot (\boldsymbol{u}_\alpha c_\alpha k_b T_\alpha) - \nabla \cdot \boldsymbol{q}_\alpha + \left[\frac{\partial w_\alpha}{\partial t}\right]_{\text{col}} \tag{3}$$

for $\alpha = 1, 2$. Repeated index α does not imply summation. In Eqs. (1)–(3), c_α is the particle concentration; $\boldsymbol{u}_\alpha$ is the particle velocity vector, $\boldsymbol{p}_\alpha$ is the particle momentum density vector; T_α is the particle temperature; w_α is the particle energy density; $\boldsymbol{q}_\alpha$ is the particle heat flux vector; ε is the magnitude of an elementary charge; k_b is the Boltzmann constant and $[\,]_{\text{col}}$ denotes the collision terms accounting for the particle–particle interactions, particle–lattice interactions, the transfer of energy between particle and lattice, and the generation and recombination process.

As noted above, Eqs. (1)–(3) represent two systems of equations corresponding to $\alpha = 1$ and $\alpha = 2$. We define the system with $\alpha = 1$ to be the equations governing the electrons, and the system with $\alpha = 2$ to be the equations governing the holes. In the sequel, Greek subscript α designates the electron and hole system according to the above stated convention and repeated Greek subscript does not imply summation. α is part of the variable symbol to emphasize the system to which it belongs.

The electron and hole concentrations are coupled to the electrostatic potential, ψ, by the Poisson equation. The Poisson equation, derived from Maxwells equations [25], is given by

$$\nabla \cdot (\theta \boldsymbol{E}) = -\varepsilon(c_1 - c_2 - N_D^+ + N_A^-) \tag{4}$$

where θ is the dielectric permittivity, N_D^+ is the concentration of the ionized donor, N_A^- is the concentration of ionized acceptor and $\boldsymbol{E}$ is the electric field vector. The electric field is related to the electrostatic potential by the equation

$$\boldsymbol{E} = -\nabla\psi \tag{5}$$

3. Hydrodynamic model

3.1. Simplification and assumptions

Eqs. (1)–(5) represent an indeterminate system of equations as the number of unknowns are more than the number of equations. In order to facilitate a solution to the device model a few constitutive approximations need to be made. The carrier momentum density vector can be represented as

$$\boldsymbol{p}_\alpha = m_\alpha c_\alpha \boldsymbol{u}_\alpha \tag{6}$$

where m_α represents the particle mass. Note that $m_1 = 0.26m_0$ and $m_2 = 0.386m_0$, where m_0 is the free electron mass. The carrier energy density can be expressed as

$$w_\alpha = \frac{3}{2} c_\alpha k_b T_\alpha + \frac{1}{2} m_\alpha c_\alpha |\boldsymbol{u}_\alpha|^2 \tag{7}$$

The heat conduction is assumed to be given by the Fourier law, i.e.

$$\boldsymbol{q}_\alpha = -\kappa_\alpha \nabla T_\alpha \tag{8}$$

The particle heat-conductivity κ_α is given by the Wiedemann–Franz law as

$$\kappa_\alpha = \left(\frac{5}{2} + \varsigma\right) \frac{\mu_{0\alpha} c_\alpha k_b^2 T_0}{\varepsilon} \tag{9}$$

where $\mu_{0\alpha}$ is the particle low-field mobility and T_0 is the lattice temperature (which is assumed to be constant in this paper). ς is a parameter associated with the energy dependence of the momentum relaxation time. In this study, $\varsigma = -2$ is employed.

The collision term, $[\partial c_\alpha / \partial t]_{\text{col}}$, in Eq. (1) describes the rate of change of particle concentration due to collisions. This term is neglected for single carrier devices, as in [1]. In the presence of both electrons and holes, this collision term has significant contribution to the transport equations and introduces coupling between the electron and hole transport systems. The collision term for the continuity equation describes the generation and recombination processes and has the following form

$$\left[\frac{\partial c_\alpha}{\partial t}\right]_{\text{col}} = G - R \tag{10}$$

where G is the avalanche generation term and R is the recombination term. The recombination term is a sum of Shockley–Read–Hall and Auger recombinations [25], i.e.

$$R = R_{\text{SRH}} + R_{\text{AU}} \tag{11}$$

The physical processes involved with the Auger recombination and the avalanche generation terms remain subjects of active investigation; these terms are not modeled in this study. The Shockley–Read–Hall recombination is given by

$$R_{\text{SRH}} = \frac{c_1 c_2 - c_{\text{int}}^2}{\tau_2(c_1 + c_{\text{int}}) + \tau_1(c_2 + c_{\text{int}})} \tag{12}$$

where c_{int} is the intrinsic carrier concentration for the silicon material, τ_1 is the electron life time and τ_2 is the hole life time and a value of 10^{-7} s is employed for both electron and hole lifetimes in this study.

The collision term, $[\partial \boldsymbol{p}_\alpha / \partial t]_{\text{col}}$, in Eq. (2) describes the particle rate of change of momentum due to collisions. This collision term can be treated by employing a relaxation time approximation [4] as

$$\left[\frac{\partial \boldsymbol{p}_\alpha}{\partial t}\right]_{\text{col}} = -\frac{\boldsymbol{p}_\alpha}{\tau_{p\alpha}} + \frac{\boldsymbol{p}_\alpha}{c_\alpha}\left[\frac{\partial c_\alpha}{\partial t}\right]_{\text{col}} \tag{13}$$

The second term in the above equation accounts for the rate of change of momentum due to particle generation and recombination processes. The validity of this term is still a subject of active investigation. This term is included in our model as an option. The simulation results presented in this paper, however, do not include this term. In Eq. (13), $\tau_{p\alpha}$ denotes the momentum relaxation time given by

$$\tau_{p\alpha} = \frac{m_\alpha \mu_{0\alpha} T_0}{\varepsilon T_\alpha} \tag{14}$$

The collision term, $[\partial w_\alpha / \partial t]_{\text{col}}$, in Eq. (3) describes the particle rate of change of energy due to collisions. This collision term can also be treated by employing relaxation time approximation as

$$\left[\frac{\partial w_\alpha}{\partial t}\right]_{\text{col}} = -\frac{(w_\alpha - w_{0\alpha})}{\tau_{w\alpha}} + \frac{w_\alpha}{c_\alpha}\left[\frac{\partial c_\alpha}{\partial t}\right]_{\text{col}} \tag{15}$$

The second term in the above equation accounts for the rate of change of energy density due to particle generation and recombination processes. Similar to the discussion on the collision term for the momentum conservation equation, our numerical results do not include this term although it can be included as an option to our model easily. In Eq. (15)

$$w_{0\alpha} = \frac{3}{2} c_\alpha k_b T_0 \tag{16}$$

denotes the equilibrium energy density and $\tau_{w\alpha}$ denotes the energy relaxation time expressed as

$$\tau_{w\alpha} = \frac{3}{2} \frac{\mu_{0\alpha}}{\varepsilon v_{s\alpha}^2} \left(\frac{k_b T_\alpha T_0}{T_\alpha + T_0} \right) + \frac{\tau_{p\alpha}}{2} \tag{17}$$

and $v_{s\alpha}$ denotes the particle saturation velocity.

3.2. Relationship to ideal gas equations

In [1] we have established the resemblance of the hydrodynamic semiconductor device equations for single carrier transport to the compressible Euler and Navier–Stokes equations of fluid dynamics. The result can be extended to the two carrier transport problem in a straightforward manner. Specifically, one can treat the electron and hole transport equations analogous to interacting flows with two different gas types. Formally, the resemblance to ideal gas equations can be stated as follows:

The αth particle/carrier hydrodynamic transport equations, without neglecting the convective terms, represent the flow of an ideal gas with the particle gas constant $R_\alpha = k_b/m_\alpha$, the ratio of specific heats $\gamma_\alpha = 5/3$, pressure $P_\alpha = c_\alpha R_\alpha T_\alpha$ and the total energy per unit mass $e_\alpha^{\text{tot}} = 1.5 R_\alpha T_\alpha + 0.5 |\boldsymbol{u}_\alpha|^2 = e_\alpha^{\text{int}} + e_\alpha^{\text{kin}}$, where e_α^{int} and e_α^{kin} denote the internal and kinetic energies per unit mass, respectively. Furthermore, the αth carrier transport equations resemble the compressible Euler equations with the addition of the heat conduction term, the collision terms and the electric field terms which couple with the Poisson equation.

3.3. System form and symmetrization

The two-carrier hydrodynamic equations stated in Eqs. (1)–(3) can be put in the form of a system of equations as

$$\boldsymbol{U}_{\alpha,t} + \boldsymbol{F}^{\text{c}}_{\alpha i,i} = \boldsymbol{F}^{\text{h}}_{\alpha i,i} + \boldsymbol{F}_\alpha \tag{18}$$

where

$$\boldsymbol{U}_\alpha = \begin{Bmatrix} U_{\alpha 1} \\ U_{\alpha 2} \\ U_{\alpha 3} \\ U_{\alpha 4} \\ U_{\alpha 5} \end{Bmatrix} = c_\alpha \begin{Bmatrix} 1 \\ u_{\alpha 1} \\ u_{\alpha 2} \\ u_{\alpha 3} \\ e_\alpha^{\text{tot}} \end{Bmatrix} \qquad \boldsymbol{F}^{\text{c}}_{\alpha i} = c_\alpha u_{\alpha i} \begin{Bmatrix} 1 \\ u_{\alpha 1} \\ u_{\alpha 2} \\ u_{\alpha 3} \\ e_\alpha^{\text{tot}} \end{Bmatrix} + P_\alpha \begin{Bmatrix} 0 \\ \delta_{1i} \\ \delta_{2i} \\ \delta_{3i} \\ u_{\alpha i} \end{Bmatrix} \tag{19}$$

$$\boldsymbol{F}^{\text{h}}_{\alpha i} = \begin{Bmatrix} 0 \\ 0 \\ 0 \\ 0 \\ -q_{\alpha i} \end{Bmatrix} \tag{20}$$

$$\boldsymbol{F}_\alpha = \begin{Bmatrix} -\dfrac{(c_1 c_2 - c_{\text{int}}^2)}{\tau_2(c_1 + c_{\text{int}}) + \tau_1(c_2 + c_{\text{int}})} \\ \dfrac{\varepsilon c_\alpha}{m_\alpha} \left[(-1)^\alpha E_1 - \dfrac{u_{\alpha 1} T_\alpha}{\mu_{0\alpha} T_0} \right] \\ \dfrac{\varepsilon c_\alpha}{m_\alpha} \left[(-1)^\alpha E_2 - \dfrac{u_{\alpha 2} T_\alpha}{\mu_{0\alpha} T_0} \right] \\ \dfrac{\varepsilon c_\alpha}{m_\alpha} \left[(-1)^\alpha E_3 - \dfrac{u_{\alpha 3} T_\alpha}{\mu_{0\alpha} T_0} \right] \\ \dfrac{1}{m_\alpha} \left[(-1)^\alpha \varepsilon c_\alpha u_{\alpha i} E_i - \dfrac{\left(c_\alpha m_\alpha e_\alpha^{\text{tot}} - \dfrac{3}{2} c_\alpha k_b T_0 \right)}{\left(\dfrac{3 \mu_{0\alpha} k_b T_\alpha T_0}{2 \varepsilon v_{s\alpha}^2 (T_\alpha + T_0)} + \dfrac{m_\alpha \mu_{0\alpha} T_0}{2 \varepsilon T_\alpha} \right)} \right] \end{Bmatrix} \tag{21}$$

It is useful to rewrite Eq. (18) in the quasi-linear form as

$$\boldsymbol{U}_{\alpha,t} + \boldsymbol{A}_{\alpha i}\boldsymbol{U}_{\alpha,i} = (\boldsymbol{K}_{\alpha ij}\boldsymbol{U}_{\alpha,j})_{,i} + \boldsymbol{F}_{\alpha} \tag{22}$$

where $\boldsymbol{A}_{\alpha i} = \boldsymbol{F}^{\mathrm{c}}_{\alpha i,\boldsymbol{U}_{\alpha}}$ and $\boldsymbol{K}_{\alpha ij}\boldsymbol{U}_{\alpha,j} = \boldsymbol{F}^{\mathrm{h}}_{\alpha i}$. The matrices $\boldsymbol{A}_{\alpha i}$ do not possess the properties of symmetry or positiveness and, in general, are functions of $\boldsymbol{U}_{\alpha}$. In the following, a brief review is presented on the symmetrization techniques for Eq. (22) as the finite element formulation based on a symmetrized form of Eq. (22) can be shown to be unconditionally stable.

Symmetrization procedures for systems of form (22) have been investigated by Harten [13]. A generalized entropy function was proposed by Hughes et al. [17] for symmetrization of compressible Euler and Navier–Stokes equations. In [1] a generalized entropy function was employed for symmetrization of electron hydrodynamic transport equations. Since the form of the advection and diffusion matrix operators is similar for both electron and hole transport equations, a function similar to the one employed for electron hydrodynamic equations can also be employed for hole hydrodynamic equations. Employing generalized entropy functions of the form

$$\mathscr{H}_{\alpha} = -c_{\alpha}s_{\alpha} \tag{23}$$

where s_{α} is the thermodynamic entropy per unit mass, a symmetrized form for Eq. (22) can be obtained as

$$\tilde{\boldsymbol{A}}_{\alpha 0}\boldsymbol{V}_{\alpha,t} + \tilde{\boldsymbol{A}}_{\alpha i}\boldsymbol{V}_{\alpha,i} = (\tilde{\boldsymbol{K}}_{\alpha ij}\boldsymbol{V}_{\alpha,j})_{,i} + \boldsymbol{F}_{\alpha} \tag{24}$$

where the matrix operators $\tilde{\boldsymbol{A}}_{\alpha i}$, $\tilde{\boldsymbol{K}}_{\alpha ij}$ are symmetric and $\tilde{\boldsymbol{A}}_{\alpha 0}$ is symmetric and positive definite. $\boldsymbol{V}_{\alpha}$ are referred to as entropy variables for particle α and are defined as

$$\boldsymbol{V}_{\alpha} = \frac{\partial \mathscr{H}_{\alpha}}{\partial \boldsymbol{U}_{\alpha}} = \frac{1}{T_{\alpha}}\begin{bmatrix} \mu_{\alpha} - \dfrac{|\boldsymbol{u}_{\alpha}|^2}{2} \\ u_{\alpha 1} \\ u_{\alpha 2} \\ u_{\alpha 3} \\ -1 \end{bmatrix} \tag{25}$$

where $\mu_{\alpha} = e^{\mathrm{int}}_{\alpha} + P_{\alpha}/c_{\alpha} - T_{\alpha}s_{\alpha}$ is the particle specific chemical potential. The specific form of s_{α} is given by

$$s_{\alpha} = c_{v\alpha}\ln\left(\frac{P_{\alpha}}{P_{0\alpha}}\left(\frac{c_{\alpha}}{c_{0\alpha}}\right)^{-\gamma_{\alpha}}\right) + s_{0\alpha} \tag{26}$$

where $c_{v\alpha}$ is the particle specific heat at constant volume and the quantities with subscript '0' denote the reference quantities. The definitions of the symmetrized matrix operators have been given in [1] for the electron hydrodynamic system. The matrix operators for hole hydrodynamic system can be defined in a similar manner by properly replacing the electron transport quantities with hole transport quantities.

4. Boundary conditions

Well-posed boundary conditions play an important role in numerical simulations. Prescribing too many boundary conditions may preclude the existence of smooth solutions. Specifying too few boundary conditions, on the other hand, may preclude uniqueness of the solution. Specification of improper number of boundary conditions can affect the convergence of the numerical schemes. Hence, it is important that one specifies the proper set of boundary conditions for numerical simulations. Well-posed boundary conditions for the classical DD model are well understood. The same set of boundary conditions, however, do not give well-posedness for the HD model. Thomann and Odeh [30] have shown that the boundary conditions based on the DD model are not sufficient for the HD model.

While they have shown that additional boundary conditions are needed for the HD model, their analysis has been focused on the 2D hydrodynamic model and for subsonic flows.

Bova and Carey [6] have reported a study on boundary conditions for HD equations, taking advantage of the resemblance of HD equations to compressible Euler and Navier–Stokes equations. The number of boundary conditions that they have proposed are identical to those specified for Euler equations. In doing so they assumed that the diffusive effect of the heat flux term on the average energy is small on the boundaries; however, this assumption lacks a physical basis. As shall be shown in this paper, the proper number of boundary conditions that need to be specified for the HD equations are not identical to those of the Euler or Navier–Stokes equations. Well-posed boundary conditions for Euler and Navier–Stokes equations have been investigated by Strikwerda [29], Gustafson and Sundstrom [12], Oliger and Sundstrom [22], among others. The concepts developed in these studies are extended to derive well-posed boundary conditions for the HD equations. In this paper an analysis is performed on the general multi-dimensional (one-, two- and three-dimensional) HD equations to include the heat flux term and to place no restriction on the type of flow, albeit subsonic or supersonic nature.

4.1. *Primitive variable form*

The two-carrier hydrodynamic equations discussed in this paper can be written in system form using primitive variables $(c_\alpha, \boldsymbol{u}_\alpha, T_\alpha)$. The primitive variables are used to analyze the number of boundary conditions that need to be specified at the inflow and outflow boundaries, that constitute a well-posed Initial Boundary Value Problem (IBVP). Using primitive variables, the conservation laws can be written using matrix-operators as

$$\frac{\partial \hat{\boldsymbol{U}}_\alpha}{\partial t} = \hat{\boldsymbol{A}}_{\alpha i}\frac{\partial \hat{\boldsymbol{U}}_\alpha}{\partial x_i} + \hat{\boldsymbol{K}}_{\alpha ij}\frac{\partial^2 \hat{\boldsymbol{U}}_\alpha}{\partial x_i x_j} + \hat{\boldsymbol{F}}_\alpha \quad \alpha = 1, 2 \tag{27}$$

where $\hat{\boldsymbol{U}}_\alpha$ denotes the primitive variables, $\hat{\boldsymbol{A}}_{\alpha i}$ denotes the advection matrices, $\hat{\boldsymbol{K}}_{\alpha ij}$ denotes the diffusion matrices and $\hat{\boldsymbol{F}}_\alpha$ denotes the source vector consisting of the collision and electric field terms. The explicit definitions of the advection matrices are given below with $\hat{\boldsymbol{U}}_\alpha = \{T_\alpha, c_\alpha, \boldsymbol{u}_\alpha\}^{\mathrm{T}}$

$$\hat{\boldsymbol{A}}_{\alpha 1} = \begin{bmatrix} -u_{\alpha 1} & 0 & -(\gamma_\alpha - 1)T_\alpha & 0 & 0 \\ 0 & -u_{\alpha 1} & -c_\alpha & 0 & 0 \\ -R_\alpha & -\dfrac{R_\alpha T_\alpha}{c_\alpha} & -u_{\alpha 1} & 0 & 0 \\ 0 & 0 & 0 & -u_{\alpha 1} & 0 \\ 0 & 0 & 0 & 0 & -u_{\alpha 1} \end{bmatrix} \tag{28}$$

$$\hat{\boldsymbol{A}}_{\alpha 2} = \begin{bmatrix} -u_{\alpha 2} & 0 & 0 & -(\gamma_\alpha - 1)T_\alpha & 0 \\ 0 & -u_{\alpha 2} & 0 & -c_\alpha & 0 \\ 0 & 0 & -u_{\alpha 2} & 0 & 0 \\ -R_\alpha & -\dfrac{R_\alpha T_\alpha}{c_\alpha} & 0 & -u_{\alpha 2} & 0 \\ 0 & 0 & 0 & 0 & -u_{\alpha 2} \end{bmatrix} \tag{29}$$

$$\hat{\boldsymbol{A}}_{\alpha 3} = \begin{bmatrix} -u_{\alpha 3} & 0 & 0 & 0 & -(\gamma_\alpha - 1)T_\alpha \\ 0 & -u_{\alpha 3} & 0 & 0 & -c_\alpha \\ 0 & 0 & -u_{\alpha 3} & 0 & 0 \\ 0 & 0 & 0 & -u_{\alpha 3} & 0 \\ -R_\alpha & -\dfrac{R_\alpha T_\alpha}{c_\alpha} & 0 & 0 & -u_{\alpha 3} \end{bmatrix} \tag{30}$$

Note that $\hat{A}_{\alpha i}$ are square but non-symmetric matrices. Similarly, the diffusion matrices can be expressed as $\hat{K}_{\alpha ij} = \hat{K}_{\alpha}\delta_{ij}$ where δ_{ij} is the kronecker delta ($\delta_{ij} = 1$ for $i = j$ and $\delta_{ij} = 0$ for $i \neq j$) and

$$\hat{K}_{\alpha} = \begin{bmatrix} \dfrac{\hat{\kappa}_{\alpha}(\gamma_{\alpha} - 1)}{c_{\alpha} m_{\alpha} R_{\alpha}} & 0 & 0 & 0 & 0 \\ 0 & 0 & 0 & 0 & 0 \\ 0 & 0 & 0 & 0 & 0 \\ 0 & 0 & 0 & 0 & 0 \\ 0 & 0 & 0 & 0 & 0 \end{bmatrix} \tag{31}$$

$\hat{K}_{\alpha ij}$ are rank-deficient matrices.

4.2. Conditions for well-posedness

The literature on well-posedness for incompletely parabolic problems dates back to 1970s. Strikwerda's thesis [29] on well-posed boundary conditions for incompletely parabolic problems addressed several issues related to the necessary and sufficient conditions for the PDE systems of form (27) to be well-posed. This work also paved way for a number of studies addressing boundary conditions for several physical problems. Of notable interest is the one by Gustafson and Sundstrom [12], addressing the issue of well-posed boundary conditions for equations of fluid dynamics and shallow water. By following the work in these two references, we extend the concepts to study the proper boundary conditions for the HD device equations, which can be considered as intermediary between Euler and Navier–Stokes (NS) equations. To derive the number of boundary conditions that need to be imposed at inflow and outflow boundaries, several results reported in [29] and [12] are utilized. The main theorems and the definitions needed are briefly stated here; interested readers are referred to the references for the proofs.

DEFINITION 1. Let $\hat{U}_{0\alpha}$ be the initial conditions to Eq. (27). The system (27) is said to be well-posed if there is a constant $\hat{C}_{\alpha}$ such that

$$\|\hat{U}_{\alpha}\| \leq \hat{C}_{\alpha}(\|\hat{U}_{0\alpha}\| + \|\hat{F}_{\alpha}\|) \tag{32}$$

Consider the incompletely parabolic system of partial differential equations given in Eq. (27) with constant coefficient matrices. The diffusion matrices $\hat{K}_{\alpha ij}$ are rank deficient with rank $1 < n$, where n is the order of the square matrices $\hat{A}_{\alpha i}$ and $\hat{K}_{\alpha ij}$. From Eq. (31), it follows that

$$\hat{K}_{\alpha ij} = \begin{bmatrix} \hat{K}^{(11)}_{\alpha ij} & \mathbf{0} \\ \mathbf{0} & \mathbf{0} \end{bmatrix} \tag{33}$$

where

$$\hat{K}^{(11)}_{\alpha ij} = \left[\frac{\hat{\kappa}_{\alpha}(\gamma_{\alpha} - 1)}{c_{\alpha} m_{\alpha} R_{\alpha}} \right]_{1 \times 1}$$

$\hat{A}_{\alpha i}$ is partitioned as

$$\hat{A}_{\alpha i} = \begin{bmatrix} \hat{A}^{(11)}_{\alpha i} & \hat{A}^{(12)}_{\alpha i} \\ \hat{A}^{(21)}_{\alpha i} & \hat{A}^{(22)}_{\alpha i} \end{bmatrix} \tag{34}$$

$\hat{U}_{\alpha}$ is also partitioned accordingly as $\hat{U}_{\alpha} = [\hat{U}_{\alpha I}, \hat{U}_{\alpha II}]^{\mathrm{T}}$ where $\hat{U}_{\alpha I} = T_{\alpha}$ and $\hat{U}_{\alpha II} = \{c_{\alpha}, \boldsymbol{u}_{\alpha}\}^{\mathrm{T}}$.

THEOREM 1 (Strikwerda [29] and Gustafson et al. [12]). System (27) is said to be well posed, if the system

$$\frac{\partial \hat{U}_{\alpha I}}{\partial t} = \hat{K}^{(11)}_{\alpha ij} \frac{\partial^2 \hat{U}_{\alpha I}}{\partial x_i x_j} \tag{35}$$

is parabolic and that the system

$$\frac{\partial \hat{U}_{\alpha II}}{\partial t} = \hat{A}^{(22)}_{\alpha i} \frac{\partial \hat{U}_{\alpha II}}{\partial x_i} \tag{36}$$

is strictly hyperbolic.

THEOREM 2 (Strikwerda [29]). Consider the initial boundary value problem for the system (27) on a half space; i.e. $x_1 \geq 0$ *and* $-\infty < x_2, x_3 < \infty$ *with constant coefficients. For the system (27) to be well-posed, the number of independent boundary conditions is given by* $r + p$, *where* r *is the rank of* $\hat{K}_{\alpha 11}$ *and* p *is the number of negative eigenvalues of* $\hat{A}^{(22)}_{\alpha 1}$.

THEOREM 3 (Strikwerda [29]). Suppose the system (27) is approximated by a set of frozen coefficient matrices. If the approximated system to (27) is well-posed, then system (27) is well-posed.

REMARKS:

(i) Gustafson and Sundstrom [12] have shown that the definition given for well-posedness in Theorem 1 is not sufficient. They illustrated the problem using examples where the conditions stated in Theorem 1 are satisfied, but the solution has an exponential growth rate. However, such exponential growth rates cannot be obtained for symmetrizable incompletely parabolic systems. Since the NS and HD equations can be symmetrized, Theorem 1 is a sufficient condition for well-posedness.

(ii) Using the result in Theorem 2, analysis will be performed for an inflow boundary parallel to the y-axis (or an electrical contact parallel to y-axis). The analysis and results apply analogously to inflow boundaries parallel to x- or z-axis.

(iii) With Theorem 3, the examination of well-posed boundary conditions can be restricted to constant coefficient systems, instead of the more general quasi-linear system of equations.

4.3. Number of independent boundary conditions for HD equations

The theorems cited above can be directly applied to determine the number of independent boundary conditions for the HD equations. In the following, the analysis is performed on the equations for the general three-dimensional problem, and the results are analogously applicable for one- and two-dimensional problems. From the matrix definitions given in Eqs. (28)–(30), it is clear that the rank of the diffusion matrix $\hat{K}_{\alpha 11}$ is one and the submatrix $\hat{A}^{(22)}_{\alpha 1}$ of the advection matrix $\hat{A}_{\alpha 1}$ is given as

$$\hat{A}^{(22)}_{\alpha 1} = \begin{bmatrix} -u_{\alpha 1} & -c_\alpha & 0 & 0 \\ -\dfrac{R_\alpha T_\alpha}{c_\alpha} & -u_{\alpha 1} & 0 & 0 \\ 0 & 0 & -u_{\alpha 1} & 0 \\ 0 & 0 & 0 & -u_{\alpha 1} \end{bmatrix} \tag{37}$$

According to Theorem 2, the number of boundary conditions can be determined by finding the number of negative eigenvalues of the above matrix. The four eigenvalues of $\hat{A}^{(22)}_{\alpha 1}$ are

$$\begin{aligned} \lambda_{\alpha 1} &= \lambda_{\alpha 2} = -u_{\alpha 1} \\ \lambda_{\alpha 3} &= -u_{\alpha 1} + C_\alpha \\ \lambda_{\alpha 4} &= -u_{\alpha 1} - C_\alpha \end{aligned} \tag{38}$$

where $C_\alpha = \sqrt{R_\alpha T_\alpha}$ is the speed of sound. From (38), the number of boundary conditions can be derived by classifying the inflow and outflow as either subsonic ($|u_{\alpha 1}| < C_\alpha$) or supersonic ($|u_{\alpha 1}| > C_\alpha$) flow:

(1) *Subsonic inflow* ($C_\alpha > u_{\alpha 1} > 0$): In this case three of the eigenvalues ($\lambda_{\alpha 1}$, $\lambda_{\alpha 2}$, $\lambda_{\alpha 4}$) of $\hat{A}^{(22)}_{\alpha 1}$ are negative. Thus a total of 4 boundary conditions are needed for the inflow to ensure well-

posedness (for the Euler and NS equations four and five boundary conditions are needed, respectively, for the inflow).

(2) *Subsonic outflow* ($0 > u_{\alpha 1} > -C_\alpha$): In this case there is only one negative eigenvalue ($\lambda_{\alpha 4}$) in $\hat{A}^{(22)}_{\alpha 1}$. Therefore, a total of two boundary conditions is needed for the outflow to ensure well-posedness of the system (for the Euler and NS equations, one and four boundary conditions are needed, respectively, for the outflow).

(3) *Supersonic inflow* ($u_{\alpha 1} > C_\alpha > 0$): In this case all four eigenvalues of $\hat{A}^{(22)}_{\alpha 1}$ are negative. We thus need to specify five boundary conditions at the inflow for a well-posed system (the Euler and NS equations also require five boundary conditions).

(4) *Supersonic outflow* ($0 > -C_\alpha > u_{\alpha 1}$): In this case all eigenvalues of $\hat{A}^{(22)}_{\alpha 1}$ are positive and we need to specify just one boundary condition at the outflow to ensure well-posedness of the system (for the Euler and NS equations, we need zero and four, boundary conditions, respectively, for the outflow).

Table 1 summarizes the number of independent boundary conditions for one-, two- and three-dimensional flows for the Euler, Navier–Stokes and HD equations. In general, we can express the number of boundary conditions in terms of the number of primitive variables (i.e. the degree of freedom n_{dof} per each node) as tabulated in Table 2. Note that $n_{\text{dof}} = n_{\text{sd}} + 2$, where n_{sd} is the number of space dimensions equal to 1, 2, 3 for 1D, 2D and 3D problems, respectively.

4.4. Specification of boundary conditions

The classical energy method can be applied to show well-posedness for symmetrizable incompletely parabolic systems. In this approach, energy growth expressions are derived by considering the variational forms for the frozen coefficient system of equations (Eqs. (24) or (27)). These expressions have been derived for Euler and Navier–Stokes equations in [12] and for the hydrodynamic device

Table 1
Number of independent boundary conditions

Type of flow	Euler	NS	HD
One-dimensional flow			
Subsonic inflow	2	3	2
Subsonic outflow	1	2	2
Supersonic inflow	3	3	3
Supersonic outflow	0	2	1
Two-dimensional flow			
Subsonic inflow	3	4	3
Subsonic outflow	1	3	2
Supersonic inflow	4	4	4
Supersonic outflow	0	3	1
Three-dimensional flow			
Subsonic inflow	4	5	4
Subsonic outflow	1	4	2
Supersonic inflow	5	5	5
Supersonic outflow	0	4	1

Table 2
Summary of independent boundary conditions for 1-, 2- and 3D flows

Type of flow	Euler	NS	HD
Subsonic inflow	$n_{\text{dof}} - 1$	n_{dof}	$n_{\text{dof}} - 1$
Subsonic outflow	1	$n_{\text{dof}} - 1$	2
Supersonic inflow	n_{dof}	n_{dof}	n_{dof}
Supersonic outflow	0	$n_{\text{dof}} - 1$	1

equations in [3]. In these references it was shown that to obtain boundedness of the solution at all times, the boundary integrals contained in the energy growth expression need to be positive, i.e.

$$\int_\Gamma V_\alpha'^{\mathrm{T}} \tilde{A}_{\alpha 1} V_\alpha' \, d\Gamma + 2 \int_\Gamma V_\alpha'^{\mathrm{T}} \tilde{K}_{\alpha 11} \frac{\partial V_\alpha'}{\partial x_1} \, d\Gamma \geq 0 \tag{39}$$

where V_α' denotes the variation of V_α. The definition for V_α' is given in Eq. (40).

$$V_\alpha' = \begin{bmatrix} -\dfrac{u_{\alpha i}}{T_\alpha} u_{\alpha i}' + \dfrac{|u_\alpha|^2}{2T_\alpha^2} T_\alpha' + R_\alpha \dfrac{c_\alpha'}{c_\alpha} - c_{v\alpha} \dfrac{T_\alpha'}{T_\alpha} \\ (T_\alpha u_{\alpha 1}' - u_{\alpha 1} T_\alpha')/T_\alpha^2 \\ (T_\alpha u_{\alpha 2}' - u_{\alpha 2} T_\alpha')/T_\alpha^2 \\ (T_\alpha u_{\alpha 3}' - u_{\alpha 3} T_\alpha')/T_\alpha^2 \\ T_\alpha'/T_\alpha^2 \end{bmatrix} \tag{40}$$

Substituting the definitions for V_α', $\tilde{A}_{\alpha 1}$ and $\tilde{K}_{\alpha 11}$, Eq. (39) can be rewritten as

$$\frac{1}{T_\alpha}\left[-c_\alpha u_{\alpha 1}\left(\sum_{i=1}^{n_{sd}} u_{\alpha i}'^2 + \frac{R_\alpha T_\alpha}{(\gamma_\alpha - 1)} \left(\frac{T_\alpha'}{T_\alpha}\right)^2 + R_\alpha T_\alpha \left(\frac{c_\alpha'}{c_\alpha}\right)^2 \right) - 2R_\alpha T_\alpha c_\alpha' u_{\alpha 1}' \right] + \frac{1}{T_\alpha}\left[-2c_\alpha R_\alpha T_\alpha' u_{\alpha 1}' + 2\frac{\hat{\kappa}_\alpha}{m_\alpha} T_\alpha' T_\alpha^{-1} \frac{\partial}{\partial x}(T_\alpha') \right] \geq 0 \tag{41}$$

The boundary conditions for HD equations are imposed by satisfying the positivity condition specified in Eq. (41). In the following, we will consider each of the four cases discussed before, i.e. subsonic/supersonic inflow and subsonic/supersonic outflow, and derive a set(s) of boundary conditions and show that these boundary conditions satisfy the inequality equation (41).

4.4.1. Subsonic inflow ($C_\alpha > u_{\alpha 1} > 0$)

From Table 2 we need to specify 2, 3 and 4 boundary conditions for 1D, 2D and 3D, respectively. One set of possible boundary conditions are summarized below

1D: $c_\alpha u_{\alpha 1} = g_{\alpha 1}$ and $T_\alpha = g_{\alpha 2}$

2D: $c_\alpha u_{\alpha 1} = g_{\alpha 1}, u_{\alpha 2} = g_{\alpha 2}$ and $T_\alpha = g_{\alpha 3}$

3D: $c_\alpha u_{\alpha 1} = g_{\alpha 1}, u_{\alpha 2} = g_{\alpha 2}, u_{\alpha 3} = g_{\alpha 3}$ and $T_\alpha = g_{\alpha 4}$

where $g_{\alpha i}$ denotes a prescribed value for the quantity to be specified. In the following, it will be verified that the boundary conditions indeed satisfy the inequality equation (41). The prescribed boundary conditions would mean $u_{\alpha 2}' = u_{\alpha 3}' = T_\alpha' = 0$. Substituting these in Eq. (41) would make the left-hand side (lhs) of the inequality equation (41) as

$$\text{lhs} = -c_\alpha u_{\alpha 1}\left(u_{\alpha 1}'^2 + R_\alpha T_\alpha \left(\frac{c_\alpha'}{c_\alpha}\right)^2 \right) - 2R_\alpha T_\alpha u_{\alpha 1}' c_\alpha' \tag{42}$$

The boundary condition $c_\alpha u_{\alpha 1} = g_{\alpha 1}$ gives $c_\alpha'/c_\alpha = -u_{\alpha 1}'/u_{\alpha 1}$. Substituting this condition into Eq. (42), we get

$$\text{lhs} = \frac{u_{\alpha 1}'^2}{g_{\alpha 1}}(-u_{\alpha 1}^2 + C_\alpha^2) > 0 \tag{43}$$

since the flow is subsonic. The boundary conditions for 1D and 2D cases can be verified in a similar manner.

A second set of boundary conditions that can be specified for subsonic inflow stems from Schottky barriers. In this type of boundary condition the normal component of current is related to the concentration. For electrons and holes, this condition is given as

$$-c_\alpha u_{\alpha 1} = v_{\text{th}}(c_\alpha - c_{0\alpha}) \tag{44}$$

where v_{th} is the thermionic velocity and $c_{0\alpha}$ is the equilibrium concentration. Using this condition, the second set of boundary conditions can be summarized as follows:

1D: $u_{\alpha 1} = -v_{th}\left(1 - \frac{c_{0\alpha}}{c_\alpha}\right)$ and $T_\alpha = g_{\alpha 2}$

2D: $u_{\alpha 1} = -v_{th}\left(1 - \frac{c_{0\alpha}}{c_\alpha}\right), u_{\alpha 2} = g_{\alpha 2}$ and $T_\alpha = g_{\alpha 3}$

3D: $u_{\alpha 1} = -v_{th}\left(1 - \frac{c_{0\alpha}}{c_\alpha}\right), u_{\alpha 2} = g_{\alpha 2}, u_{\alpha 3} = g_{\alpha 3}$ and $T_\alpha = g_{\alpha 4}$

For these boundary conditions, it can be shown that the inequality in Eq. (41) would be satisfied for the following condition

$$0 \leq u_{\alpha 1} \leq 2\left(\frac{C_\alpha^2 g_\alpha}{g_\alpha^2 + C_\alpha^2}\right) \tag{45}$$

where $g_\alpha = (v_{th} c_{0\alpha})/c_\alpha$. The first set of boundary conditions are harder to implement for device examples as the quantity $c_\alpha u_{\alpha 1}$ is not generally known.

It is to be observed that the prescribed c_α, T_α and tangential components of velocity (for multi-dimensional flows) are not well-posed boundary conditions, even though these are the commonly employed boundary conditions for device simulation. We do not suggest that the boundary conditions discussed above (and hereafter) exhaust all possible sets of boundary conditions. For instance, in the case of a high level injection of a diode, none of the above sets of boundary conditions seem to be appropriate. Development of a set of proper boundary conditions for such a device remains a subject for further investigation.

4.4.2. Subsonic outflow $(0 > u_{\alpha 1} > -C_\alpha)$

For subsonic outflow, regardless of the space dimension of the problem, two boundary conditions need to be specified. Inequality equation (41) can be satisfied by choosing any of the following three sets of boundary conditions.

1: $c_\alpha = g_{\alpha 1}$ and $T_\alpha = g_{\alpha 2}$

2: $u_{\alpha 1} = -v_{th}\left(1 - \frac{c_{0\alpha}}{c_\alpha}\right)$ and $T_\alpha = g_{\alpha 2}$

3: $u_{\alpha 1} = g_{\alpha 3}$ and $\frac{\partial T_\alpha}{\partial x} = g_{\alpha 4}$

In semiconductor device simulation, the inflow velocity $u_{\alpha 1}$ is typically not known. So the first two sets of boundary conditions are more appropriate compared to the third set. For the first set of boundary conditions the inequality is satisfied, i.e.

$$-c_\alpha u_{\alpha 1}\left(\sum_{i=1}^{n_{sd}} u_{\alpha i}'^2 + \frac{R_\alpha T_\alpha}{(\gamma_\alpha - 1)}\left(\frac{T_\alpha'}{T_\alpha}\right)^2 + R_\alpha T_\alpha\left(\frac{c_\alpha'}{c_\alpha}\right)^2\right) > 0 \tag{46}$$

since $u_{\alpha 1} < 0$ and the quantity inside the parenthesis is positive. In the second set of boundary conditions (again based on Schottky barrier), a velocity boundary condition similar to the one suggested for subsonic inflow is employed. In this case the inequality takes the form

$$-c_\alpha u_{\alpha 1}\left(\sum_{i=1}^{n_{sd}} u_{\alpha i}'^2 + \frac{R_\alpha T_\alpha}{(\gamma_\alpha - 1)}\left(\frac{T_\alpha'}{T_\alpha}\right)^2 + R_\alpha T_\alpha\left(\frac{c_\alpha'}{c_\alpha}\right)^2\right) + \frac{2R_\alpha T_\alpha v_{th} c_{0\alpha}}{c_\alpha^2} c_\alpha'^2 \geq 0 \tag{47}$$

since $u_{\alpha 1} < 0$. Note that for this set of boundary conditions no limit is placed on the inflow velocity $u_{\alpha 1}$.

Commonly employed boundary conditions for 2D simulations (assume the contact placement is parallel to x-axis) are $c_\alpha = g_{\alpha 1}$, $u_{\alpha 2} = 0$ and $T_\alpha = g_{\alpha 3}$. Based on the above development this set of boundary conditions appears to be an over specification.

4.4.3. Supersonic inflow ($u_{\alpha 1} < C_\alpha > 0$)

For supersonic inflow one needs to specify 3, 4 and 5 boundary conditions for 1D, 2D and 3D problems, respectively. The number of conditions would imply that all the basic nodal variables be specified. So the following set of boundary conditions can be specified

$$T_\alpha = g_{\alpha n_{\mathrm{sd}}+2}, c_\alpha = g_{\alpha;1}, \quad \text{and} \quad u_{\alpha;i} = g_{\alpha;i+1} \text{ for } i = 1, n_{\mathrm{sd}}$$

The boundary conditions mentioned here pose an interesting physical question. As noted earlier, the inflow velocity is typically not known, i.e. $u_{\alpha 1}$ is not know. However, since the flow is supersonic we may impose that the inflow velocity cannot be greater than the saturation velocity. Alternatively, any other set of boundary conditions that satisfies the inequality (41) are also applicable. For the boundary conditions specified above, the left-hand side of Eq. (41) is equal to zero. It should be mentioned that in semiconductor device simulation, supersonic inflow boundaries are rarely encountered.

4.4.4. Supersonic outflow ($0 > -C_\alpha > u_{\alpha 1}$)

Independent of the space dimension, only one boundary condition needs to be specified for this case. Valid boundary conditions include setting $\partial T_\alpha / \partial x = g_{\alpha 1}$ or $T_\alpha = g_{\alpha 2}$. In this case the inequality takes the form

$$\mathrm{lhs} = -c_\alpha u_{\alpha 1}\left(\sum_{i=1}^{n_{\mathrm{sd}}} u_{\alpha i}'^2 + \frac{R_\alpha T_\alpha}{(\gamma_\alpha - 1)}\left(\frac{T_\alpha'}{T_\alpha}\right)^2 + R_\alpha T_\alpha\left(\frac{c_\alpha'}{c_\alpha}\right)^2\right) - 2R_\alpha T_\alpha c_\alpha' u_{\alpha 1}' - 2c_\alpha R_\alpha T_\alpha' u_{\alpha 1}' \tag{48}$$

This equation can be rewritten as

$$\begin{aligned}\mathrm{lhs} = {} & -c_\alpha u_{\alpha 1}\left(\sum_{i=2}^{n_{\mathrm{sd}}} u_{\alpha i}'^2\right) - \frac{u_{\alpha 1} c_\alpha R_\alpha T_\alpha}{\gamma_\alpha(\gamma_\alpha - 1)}\left[\left(\frac{T_\alpha'}{T_\alpha} - (\gamma_\alpha - 1)\frac{c_\alpha'}{c_\alpha}\right)^2\right] \\ & + \frac{1}{2}(-u_{\alpha 1} - C_\alpha)c_\alpha\left[u_{\alpha 1}' + \sqrt{\frac{R_\alpha T_\alpha}{\gamma_\alpha}}\left(\frac{T_\alpha'}{T_\alpha} + \frac{c_\alpha'}{c_\alpha}\right)\right]^2 \\ & + \frac{1}{2}(-u_{\alpha 1} + C_\alpha)c_\alpha\left[u_{\alpha 1}' - \sqrt{\frac{R_\alpha T_\alpha}{\gamma_\alpha}}\left(\frac{T_\alpha'}{T_\alpha} + \frac{c_\alpha'}{c_\alpha}\right)\right]^2\end{aligned} \tag{49}$$

In this case $u_{\alpha 1} < 0$ and both $(-u_{\alpha 1} - C_\alpha)$ and $(-u_{\alpha 1} + C_\alpha)$ are positive; hence the inequality (41) is satisfied.

REMARKS:

(i) The examples for inflow and outflow boundaries and subsonic/supersonic cases are representatives of the possible sets of well-posed boundary conditions for the HD system. The boundary conditions discussed have either physical or mathematical basis and can easily be implemented.

(ii) Mixed type of boundary conditions (involving the quantity and its derivative) are among the feasible sets of boundary conditions. Reference [12] has some examples on this type for Euler and Navier–Stokes equations. Mixed type of boundary conditions are not presented here since they are usually more difficult to implement.

(iii) In practice, simulations are performed without verifying the well-posedness of the boundary conditions. If stable numerical schemes are employed, exponential growth in the solution can be avoided. However, where possible it is recommended that well-posed boundary conditions be specified to avoid steep gradients in the solution and to ensure the convergence behavior of the numerical scheme.

5. Numerical scheme for two-carrier hydrodynamic equations

The most common numerical schemes employed for semiconductor device simulation are finite difference and finite volume based schemes. See [23, 25] for an overview of finite difference or volume

based schemes for drift diffusion equations, [7] for the extension of these schemes to energy transport equations and [8, 9] for the application of difference based schemes to hydrodynamic equations.

Finite element methods have not been attempted with much success to device simulation [25] as the standard Galerkin finite element method exhibits spurious oscillations when the exact solution contains steep layers. Hughes and Brooks developed a Streamline Upwind Petrov–Galerkin (SUPG) [15] finite element method which can resolve steep layers in the exact solution efficiently. Sharma and Carey [28] implemented this SUPG finite element formulation for the traditional drift diffusion equations. Hughes et al. [16–18, 26, 27] generalized the SUPG finite element formulation to Galerkin/least-squares finite element formulation and successfully applied it to compressible and incompressible behavior of fluids, In [1], a Galerkin/least-squares finite element formulation is applied to treat the single carrier hydrodynamic semiconductor device equations. In Galerkin/least-squares finite element formulation terms of a least-squares type are added to the variational equation obtained from the Galerkin method. These least-squares terms vanish when the exact solution is obtained, thus making it a consistent method. GLS is a higher order accurate method with good stability properties. The temporal behavior of the HD equations is discretized using a discontinuous Galerkin method in time [19]. This discretization consists of a constant-in-time approximation, which leads to an inexpensive and highly stable first-order time-accurate algorithm, ideal for steady problems.

In this section the details on extending the Galerkin/least-squares formulation to two-carrier hydrodynamic device equations are presented.

5.1. *Variational forms for the hydrodynamic equations*

Let the variational function spaces $\mathcal{S}_n$ and ϑ_n both consist of continuous functions with square integrable first derivatives within each space–time slab. The solution space $\mathcal{S}_n$ is the set of all such functions satisfying the essential boundary conditions. While the weighting function space, ϑ_n, is made up of functions whose value is zero where essential boundary conditions are specified, i.e.

$$\begin{aligned} \mathcal{S}_n &= \{\boldsymbol{V}_\alpha \mid \boldsymbol{V}_\alpha \in H^1(Q_n), \boldsymbol{D}_\alpha(\boldsymbol{V}_\alpha) = \boldsymbol{g}_\alpha(t) \text{ on } B_n\} \\ \vartheta_n &= \{\boldsymbol{W}_\alpha \mid \boldsymbol{W}_\alpha \in H^1(Q_n), \boldsymbol{D}'_\alpha(\boldsymbol{W}_\alpha) = 0 \text{ on } B_n\} \end{aligned} \tag{50}$$

where $Q_n = \Omega \times I_n$ is the space–time slab with boundary $B_n = \Gamma \times I_n$. $\boldsymbol{D}_\alpha$ and $\boldsymbol{D}'_\alpha$ denote the nonlinear boundary condition operators for the αth carrier and $\boldsymbol{g}_\alpha$ denotes the vector of prescribed boundary conditions. Ω denotes the multi-dimensional spatial domain with boundary Γ and $I_n =]t_n, t_{n+1}[$ denotes the nth time interval with t_n and t_{n+1} as the nth and $(n+1)$th time levels, respectively. Before stating the weak form, it is useful to introduce the following notation:

$$(\boldsymbol{W}_\alpha, \boldsymbol{V}_\alpha)_{Q_n} = \int_{Q_n} (\boldsymbol{W}_\alpha \cdot \boldsymbol{V}_\alpha)\, \mathrm{d}Q \tag{51}$$

$$(\boldsymbol{W}_\alpha, \boldsymbol{V}_\alpha)_{\Omega} = \int_{\Omega} (\boldsymbol{W}_\alpha \cdot \boldsymbol{V}_\alpha)\, \mathrm{d}\Omega \tag{52}$$

$$a(\boldsymbol{W}_\alpha, \boldsymbol{V}_\alpha)_{Q_n} = \int_{Q_n} (\boldsymbol{W}_{\alpha,i} \cdot \tilde{\boldsymbol{K}}_{\alpha ij} \boldsymbol{V}_{\alpha,i})\, \mathrm{d}Q \tag{53}$$

$$(\boldsymbol{W}_\alpha, \boldsymbol{V}_\alpha)_{B_n} = \int_{B_n} (\boldsymbol{W}_\alpha \cdot \boldsymbol{V}_\alpha) n_i\, \mathrm{d}B \tag{54}$$

$$(\boldsymbol{W}_\alpha, \boldsymbol{V}_\alpha)_{Q_n^{\mathrm{e}}} = \sum_{e=1}^{(n_{\mathrm{el}})_n} \int_{Q_n^{\mathrm{e}}} (\boldsymbol{W}_\alpha \cdot \boldsymbol{V}_\alpha)\, \mathrm{d}Q \tag{55}$$

In Eq. (55), $(n_{\mathrm{el}})_n$ denotes the number of space–time finite elements at time level n, $Q_n^{\mathrm{e}} = \Omega_n^{\mathrm{e}} \times I_n$ denotes the domain of element interior, and n_i denotes the unit outward normal. Note that the operators defined in Eqs. (51)–(55) are symmetric, i.e. $(\boldsymbol{W}_\alpha, \boldsymbol{V}_\alpha)_\Omega = (\boldsymbol{V}_\alpha, \boldsymbol{W}_\alpha)_\Omega$.

The weak form can be stated as follows: Within each Q_n, $n = 0, \ldots, N-1$, find $v_\alpha \in S_n$ such that for all $W_\alpha \in \vartheta_n$ the following variational equation is satisfied

$$B(W_\alpha, V_\alpha)_{\alpha n} = L(W_\alpha)_{\alpha n} \tag{56}$$

where

$$\begin{aligned} B(W_\alpha, V_\alpha)_{\alpha n} = {} & ((-W_{\alpha,t}), U_\alpha(V_\alpha))_{Q_n} - ((W_{\alpha,i}), F^{c}_{\alpha i}(\mathbf{V}_\alpha))_{Q_n} + a(W_\alpha, V_\alpha)_{Q_n} \\ & - (W_\alpha, F_\alpha(V_\alpha))_{Q_n} + (W_\alpha(t^-_{n+1}), U_\alpha(V_\alpha(t^-_{n+1})))_\Omega + (W_\alpha, F^{c}_{\alpha i}(V_\alpha) - F^{h}_{\alpha i}(V_\alpha))_{B_n} \end{aligned} \tag{57}$$

and

$$L(W_\alpha)_{\alpha n} = (W_\alpha(t^+_n), U_\alpha(V_\alpha(t^+_n)))_\Omega \tag{58}$$

Eqs. (57) and (58) are obtained by multiplying Eq. (18) with the weighting function and performing integration by parts. It is to be observed that the operator B in Eq. (56) is non-symmetric.

Let S^h_n and ϑ^h_n be the finite-dimensional approximations to S_n and ϑ_n, respectively. The time-discontinuous Galerkin formulation can be written as follows:
Within each Q_n, $n = 0, \ldots, N-1$, find $V^h_\alpha \in S^h_n$ such that for all $W^h_\alpha \in \vartheta^h_n$ the following variational equation is satisfied

$$B_{\mathrm{GAL}}(W^h_\alpha, V^h_\alpha)_{\alpha n} = L_{\mathrm{GAL}}(W^h_\alpha)_{\alpha n} \tag{59}$$

where

$$\begin{aligned} B_{\mathrm{GAL}}(W^h_\alpha, V^h_\alpha)_{\alpha n} &= B(W^h_\alpha, V^h_\alpha)_{\alpha n} \\ L_{\mathrm{GAL}}(W^h_\alpha)_{\alpha n} &= (W^h_\alpha(t^+_n), U_\alpha(V^h_\alpha(t^-_n))) \end{aligned} \tag{60}$$

A jump condition terms of the following form

$$\int_\Omega W^h_\alpha(t^+_n) \cdot \lceil \lfloor U_\alpha(V^h_\alpha(t_n)) \rfloor \rceil \, \mathrm{d}\Omega \tag{61}$$

is added to the variational equation to enforce weak initial conditions for each space–time slab. The term

$$\lceil \lfloor U_\alpha(t_n) \rfloor \rceil = U_\alpha(t^+_n) - U_\alpha(t^-_n) \tag{62}$$

denotes the jump in time of U_α in the time slab.

The Galerkin finite element formulation summarized in Eq. (59) possess poor stability properties when the global solution has steep gradients. Spurious oscillations are often observed in the vicinity of steep layers. In the following a time-discontinuous Galerkin/least-squares formulation is developed which possess improved stability properties as well as robustness.

5.2. *Time-discontinuous Galerkin/least-squares formulation*

The space–time Galerkin/least-squares finite element formulation for the αth carrier hydrodynamic transport equations can be stated as follows:
Within each Q_n, $n = 0, \ldots, N-1$, find $V^h_\alpha \in S^h_n$ such that for all $W^h_\alpha \in \vartheta^h_n$ the following variational equation is satisfied

$$B_{\mathrm{GLS}}(W^h_\alpha, V^h_\alpha)_{\alpha n} = L_{\mathrm{GLS}}(W^h_\alpha)_{\alpha n} \tag{63}$$

where

$$B_{\mathrm{GLS}}(W^h_\alpha, V^h_\alpha)_{\alpha n} = B_{\mathrm{GAL}}(W^h_\alpha, V^h_\alpha)_{\alpha n} + (\mathscr{L}_\alpha W^h_\alpha, \tau_{\mathrm{GLS}\alpha} \mathscr{L}_\alpha V^h_\alpha)_{Q^\Sigma_n} \tag{64}$$

$$L_{\mathrm{GLS}}(W^h_\alpha)_{\alpha n} = L_{\mathrm{GAL}}(W^h_\alpha)_{\alpha n} \tag{65}$$

The stability emanates from the addition of a least-squares term to the Galerkin formulation

$$\sum_{e=1}^{(n_{el})_n} \int_{Q_n^e} (\mathscr{L}_\alpha \boldsymbol{W}_\alpha^h) \cdot \tau_{GLS\alpha} (\mathscr{L}_\alpha \boldsymbol{V}_\alpha^h) \, dQ \tag{66}$$

The least-squares term is proportional to the residual and therefore only contributes to regions where the Galerkin method fails to resolve the transport of carriers. The governing differential operator, $\mathscr{L}_\alpha$ is given by

$$\mathscr{L}_\alpha = \tilde{\boldsymbol{A}}_{\alpha 0} \frac{\partial}{\partial t} + \tilde{\boldsymbol{A}}_{\alpha i} \frac{\partial}{\partial x_i} - \frac{\partial}{\partial x_i} \left(\tilde{\boldsymbol{K}}_{\alpha ij} \frac{\partial}{\partial x_j} \right) + \tilde{\boldsymbol{C}}_\alpha \tag{67}$$

where $\tilde{\boldsymbol{C}}_\alpha$ is a non-unique operator and is defined as

$$\boldsymbol{F}_\alpha = -\tilde{\boldsymbol{C}}_\alpha \boldsymbol{V}_\alpha \tag{68}$$

$\tau_{GLS\alpha}$ is an $n_{dof} \times n_{dof}$ symmetric positive-semidefinite matrix of intrinsic time scales. This is discussed in greater detail in the next sub-section.

Finite element discretization

The finite element interpolation is introduced

$$\boldsymbol{V}_\alpha^h = \sum_{A=1}^{(n_{np})_n} N_A^{(n)}(x) \boldsymbol{v}_{\alpha A}^{(n+1)} \tag{69}$$

where $\boldsymbol{v}_{\alpha A}^{(n+1)}$ are αth carriers $n_{dof} \times 1$ nodal unknowns, $N_A^{(n)}(x)$ is the matrix of shape functions for nth space–time slab and $(n_{np})_n$ is the number of finite element nodes for the nth space–time slab. As in the Galerkin finite element method, the weighting functions are interpolated using the same functions $N_A^{(n)}(x)$, i.e.

$$\boldsymbol{W}_\alpha^h = \sum_{A=1}^{(n_{np})_n} N_A^{(n)}(x) \boldsymbol{w}_{\alpha A}^{(n+1)} \tag{70}$$

Substituting the finite element interpolants, Eqs. (69) and (70), into the Galerkin/least-squares variational equation, Eq. (63), a non-linear systems of equations is obtained

$$\boldsymbol{G}_\alpha(\boldsymbol{v}_\alpha; \boldsymbol{v}_1^{(n)}; \boldsymbol{v}_2^{(n)}) = 0 \tag{71}$$

Eq. (71) means that the non-linear algebraic equations to be solved at time-level $(n+1)$ for the αth carrier, $\boldsymbol{G}_\alpha$, are a function of the αth carrier entropy variables at time-level $(n+1)$ and the electron and hole entropy variables at time-level n, $\boldsymbol{v}_1^{(n)}$ and $\boldsymbol{v}_2^{(n)}$, respectively. The non-linear system of equations can be solved by linearizing Eq. (71) with respect to the unknown variables $\boldsymbol{v}_\alpha$ and applying a time-stepping algorithm in the format of a predictor multi-corrector algorithm [1, 26].

5.2.1. Design of intrinsic time scales matrix: τ_{GLS}

A design of the time scales matrix τ_{GLS} for non-linear hydrodynamic equations is very complicated. Generally, simpler one-dimensional scalar equations are used as model problems and the results obtained from the analysis of the one-dimensional model problems are extended to multi-dimensional systems. Definitions provided for multi-dimensional systems are not necessarily optimal. Hughes et al. [18] have examined such approach to the modeling of several fluid flow problems and they showed that excellent results can be obtained when one-dimensional results are extended to non-liner multi-dimensional problems. Employing a similar approach, we consider the following scalar one-dimensional advection-diffusion equation with source term

$$u\varphi_{,x} = k\varphi_{,xx} + c_s\varphi \tag{72}$$

Following the conditions given by Shakib [26], a τ for the scalar advection–diffusion equation with source term can be written as

$$\tau_s = \left(c_s^2 + \left(2\frac{u}{h}\right)^2 + \left(\frac{4k}{h^2}\right)^2\right)^{-0.5} \tag{73}$$

where the subscript s denotes the scalar equation and h is the mesh size parameter. Eq. (73) can be rewritten as

$$\tau_s = \frac{h}{2u} \cdot \sqrt{\frac{\alpha_s^2}{1+\alpha_s^2}} \cdot \left(1 + c_s^2 \left(\frac{h}{2u}\right)^2 \frac{\alpha_s^2}{1+\alpha_s^2}\right)^{-0.5} \tag{74}$$

where $\alpha_s = uh/2k$. In Eq. (74), the first term in the product of three terms can be considered as the design of τ for advection limit case (i.e. in the absence of diffusion and source) and the next two terms can be viewed as the corrections for the presence of diffusion and source terms, respectively. More optimal definitions of τ can be derived for Eq. (72). However, they are more expensive and the gain is often little. The result obtained in Eq. (74) can be generalized to the system of equations as discussed in the following:

Consider a constant-coefficient one-dimensional system of equations in the hydrodynamic form, i.e.

$$\boldsymbol{U}_{,t} + \boldsymbol{A}\boldsymbol{U}_{,x} = \boldsymbol{K}\boldsymbol{U}_{,xx} + \boldsymbol{F} \tag{75}$$

Employing a change of variables, a symmetric system of equations can be obtained

$$\tilde{\boldsymbol{A}}_0 \boldsymbol{V}_{,t} + \tilde{\boldsymbol{A}}\boldsymbol{V}_{,x} = \tilde{\boldsymbol{K}}\boldsymbol{V}_{,xx} + \tilde{\boldsymbol{F}} \tag{76}$$

$\tilde{\boldsymbol{A}}_0$ is constant matrix and can be expressed in a product form as $\tilde{\boldsymbol{A}}_0 = \boldsymbol{L}\boldsymbol{L}^{\mathrm{T}}$. Defining $\boldsymbol{X} = \boldsymbol{L}^{\mathrm{T}}\boldsymbol{V}$, Eq. (76) can be transformed into a new system of equations

$$\boldsymbol{X}_{,t} + \bar{\boldsymbol{A}}\boldsymbol{X}_{,x} = \bar{\boldsymbol{K}}\boldsymbol{X}_{,xx} + \bar{\boldsymbol{F}} \tag{77}$$

where $\bar{\boldsymbol{A}} = \boldsymbol{L}^{-1}\tilde{\boldsymbol{A}}\boldsymbol{L}^{-\mathrm{T}}$, $\bar{\boldsymbol{K}} = \boldsymbol{L}^{-1}\tilde{\boldsymbol{K}}\boldsymbol{L}^{-\mathrm{T}}$ and $\bar{\boldsymbol{F}} = \boldsymbol{L}^{-1}\tilde{\boldsymbol{F}}$. The eigenvalues for the three systems of Eqs. (75)–(77), are identical. If we denote the eigenvectors to be Ψ, Φ and ν for Eqs. (75), (76) and (77), respectively, then the following relation holds

$$\Psi = \tilde{\boldsymbol{A}}_0 \Phi = \boldsymbol{L}(\boldsymbol{L}^{\mathrm{T}}\Phi) = \boldsymbol{L}\boldsymbol{Y} \tag{78}$$

Defining $\boldsymbol{X} = \boldsymbol{Y}\chi$, where $\boldsymbol{Y} = [\nu_1, \ldots, \nu_m]$ Eq. (77) becomes

$$\boldsymbol{Y}\chi_{,t} + \bar{\boldsymbol{A}}\boldsymbol{Y}\chi_{,x} = \bar{\boldsymbol{K}}\boldsymbol{Y}\chi_{,xx} + \bar{\boldsymbol{F}} \tag{79}$$

where $\bar{\boldsymbol{A}} = \boldsymbol{Y}\Lambda\boldsymbol{Y}^{-1}$ and $\Lambda = \mathrm{diag}[\lambda_1, \ldots, \lambda_m]$. Multiplying Eq. (79) by $\boldsymbol{Y}^{\mathrm{T}}$, from the left, one obtains

$$\chi_{,t} + \Lambda\chi_{,x} = \boldsymbol{Y}^{\mathrm{T}}\bar{\boldsymbol{K}}\boldsymbol{Y}\chi_{,xx} + \boldsymbol{Y}^{\mathrm{T}}\bar{\boldsymbol{F}} \tag{80}$$

The similarity transformation discussed above diagonalizes only the $\bar{\boldsymbol{A}}$ matrix but not the diffusion and source matrices. More general transformation procedures can be considered to diagonalize more than one matrix at a time, but the procedures are more expensive. The term τ defined using the above procedure is generally sufficient to obtain a stable and robust finite element method.

The ith scalar component of Eq. (80) can be written as

$$\chi_{i,t} + \lambda_i \chi_{i,x} = k_i \chi_{i,xx} + c_{si}\chi_i \tag{81}$$

where $k_i = \boldsymbol{Y}_i^{\mathrm{T}}\bar{\boldsymbol{K}}\boldsymbol{Y}_i = \Phi_i^{\mathrm{T}}\tilde{\boldsymbol{K}}\Phi_i$ and $c_{si} = -\Phi_i^{\mathrm{T}}\tilde{\boldsymbol{C}}\Phi_i$. Eq. (81) is similar to the scalar advection–diffusion equation considered in Eq. (72) and the two equations are in fact identical for steady-state problems. A τ_{si} (subscript si denotes the ith scalar equation) can then be defined for Eq. (81) (analogous to Eq. (73)). The intrinsic time scales matrix can now be defined by considering a Galerkin/least-squares formulation for Eq. (77) and diagonalizing the variational equations using the transformation procedure discussed in [18]. This procedure leads to the definition of τ as

$$\tau_{\mathrm{GLS}} = \Phi\ \mathrm{diag}(\tau_{s1}, \ldots, \tau_{si}, \ldots, \tau_{sm})\Phi^{\mathrm{T}} \tag{82}$$

where τ_{si} is the definition for scalar equation given in Eq. (81). For two carrier hydrodynamic equations, Eq. (82) can be generalized as

$$\tau_{\mathrm{GLS}\alpha} = \Phi_\alpha \,\mathrm{diag}(\tau_{\mathrm{GLS}\alpha 1}, \ldots, \tau_{\mathrm{GLS}\alpha m}) \Phi_\alpha^{\mathrm{T}} \tag{83}$$

5.2.2. Consistency

The consistency of the Galerkin/least-squares formulation, Eq. (63), with the strong form of the boundary value problem may be verified by replacing $\boldsymbol{V}_\alpha^h$ by $\boldsymbol{V}_\alpha$, i.e.

$$\boldsymbol{B}_{\mathrm{GLS}}(\boldsymbol{W}_\alpha^h, \boldsymbol{V}_\alpha)_{n\alpha} - \boldsymbol{L}_{\mathrm{GLS}}(\boldsymbol{W}_\alpha^h)_{n\alpha} = 0 \tag{84}$$

Substituting the expressions for $\boldsymbol{B}_{\mathrm{GLS}}$ and $\boldsymbol{L}_{\mathrm{GLS}}$ (Eq. (59)) into Eq. (84) and integrating by parts, we obtain

$$\int_{Q_n} \boldsymbol{W}_\alpha^h \cdot [\boldsymbol{U}_{\alpha,t}(\boldsymbol{V}_\alpha) + \boldsymbol{F}^{\mathrm{c}}_{\alpha i,i}(\boldsymbol{V}_\alpha) - \boldsymbol{F}^{\mathrm{h}}_{\alpha i,i}(\boldsymbol{V}_\alpha) - \boldsymbol{F}_\alpha(\boldsymbol{V}_\alpha)]\, \mathrm{d}Q$$
$$+ \int_\Omega \boldsymbol{W}_\alpha^h(t_n^+) \cdot [\![\boldsymbol{U}_\alpha(\boldsymbol{V}_\alpha(t_n))]\!]\, \mathrm{d}\Omega + \int_{Q_n} (\mathscr{L}_\alpha \boldsymbol{W}_\alpha^h) \cdot \tau_\alpha(\mathscr{L}_\alpha \boldsymbol{V}_\alpha)\, \mathrm{d}Q = 0 \tag{85}$$

Since $\boldsymbol{V}_\alpha$ is the exact solution and is smooth, the residual and the jump term are exactly zero, i.e.

$$\mathscr{L}_\alpha \boldsymbol{V}_\alpha = 0 \tag{86}$$

$$[\![\boldsymbol{U}_\alpha(\boldsymbol{V}_\alpha(t_n))]\!] = 0 \tag{87}$$

Since $\boldsymbol{W}_\alpha^h$ is arbitrary, Eq. (85) can be rewritten as

$$\boldsymbol{U}_{\alpha,t}(\boldsymbol{V}_\alpha) + \boldsymbol{F}^{\mathrm{c}}_{\alpha i,i}(\boldsymbol{V}) - \boldsymbol{F}^{\mathrm{h}}_{\alpha i,i}(\boldsymbol{V}) - \boldsymbol{F}_\alpha(\boldsymbol{V}) = 0 \tag{88}$$

which is the strong form of the problem stated in Eq. (18).

5.2.3. Entropy production: stability analysis

In this section the hydrodynamic conservation laws are analyzed for stability. Stability of the numerical algorithms is vital for numerical calculations. It is a well known fact that the Clausius–Duhem inequality provides the conditions for physical stability of the system under consideration. It is crucial that the numerical algorithms obey these stability conditions. In the following, it will be established that the numerical algorithms discussed in this paper obey these stability conditions.

Clausius–Duhem inequality

In non-equilibrium thermodynamics, the balance equation for entropy reveals that the entropy of a volume element changes with time for two reasons: (1) entropy flows into the volume element and (2) there is an entropy source due to irreversible phenomena inside the volume element. The entropy source is always a non-negative quantity, since entropy can only be created, never destroyed. For reversible transformations the entropy source vanishes. This is the local formulation of the second law of thermodynamics. By combining the second law of thermodynamics with the macroscopic laws of conservation of mass, momentum and energy an expression for the rate of change of the local entropy can be obtained [21].

The conservation laws contain a number of quantities such as the diffusion flows, the heat flow and the pressure tensor, which are related to the transport of mass, momentum and energy. The entropy source may then be calculated if one makes use of the Gibbs relation which connects the rate of change of entropy in each mass element to the rate of change of energy and the rates of change in composition. The Gibbs equation relating the entropy to the other properties of the system is given by

$$T_\alpha \,\mathrm{d}s_\alpha = \mathrm{d}e_\alpha^{\mathrm{int}} + P_\alpha \,\mathrm{d}v_\alpha \tag{89}$$

In the following, a stability condition will be derived by appropriately modifying the conservation laws.

The equation for the conservation of momentum can be modified to obtain a balance equation for the

creation of kinetic energy. Multiplying the momentum conservation equation by a velocity component $u_{\alpha i}$ and summing over all i the balance equation is obtained as

$$c_\alpha \frac{\partial}{\partial t}\left(\frac{|\boldsymbol{u}_\alpha|}{2}\right)^2 + c_\alpha u_{\alpha i}\frac{\partial}{\partial x_i}\left(\frac{|\boldsymbol{u}_\alpha|^2}{2}\right) + u_{\alpha i}\frac{\partial P_\alpha}{\partial x_i} = (-1)^\alpha \frac{\varepsilon}{m_\alpha} c_\alpha u_{\alpha i} E_i - |\boldsymbol{u}_\alpha|^2\left[\frac{\partial c_\alpha}{\partial t}\right]_{\text{col}} + \frac{u_{\alpha i}}{m_\alpha}\left[\frac{\partial p_{\alpha i}}{\partial t}\right]_{\text{col}} \tag{90}$$

Notice that the equation for conservation of particle number is utilized to obtain (90). In Eq. (90), $[\partial p_{\alpha i}/\partial t]_{\text{col}}$ denotes the ith component of the collision term for the momentum equation. Subtracting the kinetic energy expression (90) from the energy conservation equation gives

$$c_\alpha \frac{\partial e_\alpha^{\text{int}}}{\partial t} + c_\alpha u_{\alpha i}\frac{\partial e_\alpha^{\text{int}}}{\partial x_i} + P_\alpha \frac{\partial u_{\alpha i}}{\partial x_i} + \left(e_\alpha^{\text{int}} - \frac{|\boldsymbol{u}_\alpha|^2}{2}\right)\left[\frac{\partial c_\alpha}{\partial t}\right]_{\text{col}} + \frac{u_{\alpha i}}{m_\alpha}\left[\frac{\partial p_{\alpha i}}{\partial t}\right]_{\text{col}} - \frac{1}{m_\alpha}\left[\frac{\partial w_\alpha}{\partial t}\right]_{\text{col}} = -\frac{\partial q_{\alpha i}}{\partial x_i} \tag{91}$$

Eq. (91) can be rewritten as

$$c_\alpha\left(\frac{\partial e_\alpha^{\text{int}}}{\partial t} + P_\alpha \frac{\partial v_\alpha}{\partial t}\right) + c_\alpha u_{\alpha i}\left(\frac{\partial e_\alpha^{\text{int}}}{\partial x_i} + P_\alpha \frac{\partial v_\alpha}{\partial x_i}\right) + \left(h_\alpha - \frac{|\boldsymbol{u}_\alpha|^2}{2}\right)\left[\frac{\partial c_\alpha}{\partial t}\right]_{\text{col}} + \frac{u_{\alpha i}}{m_\alpha}\left[\frac{\partial p_{\alpha i}}{\partial t}\right]_{\text{col}} - \frac{1}{m_\alpha}\left[\frac{\partial w_\alpha}{\partial t}\right]_{\text{col}} = -\frac{\partial q_{\alpha i}}{\chi_i} \tag{92}$$

where $v_\alpha = 1/c_\alpha$ is the specific volume and $h_\alpha = e_\alpha^{\text{int}} + P_\alpha v_\alpha$ is the specific enthalpy.

Using Gibbs relation, Eq. (92) can be rewritten as

$$T_\alpha c_\alpha \frac{\partial s_\alpha}{\partial t} + T_\alpha c_\alpha u_{\alpha i}\frac{\partial s_\alpha}{\partial x_i} + \left(h_\alpha - \frac{|\boldsymbol{u}_\alpha|^2}{2}\right)\left[\frac{\partial c_\alpha}{\partial t}\right]_{\text{col}} + \frac{u_{\alpha i}}{m_\alpha}\left[\frac{\partial w_\alpha}{\partial t}\right]_{\text{col}} - \frac{1}{m_\alpha}\left[\frac{\partial p_{\alpha i}}{\partial t}\right]_{\text{col}} = -\frac{\partial q_{\alpha i}}{\partial x_i} \tag{93}$$

Considering the Fourier heat conduction law $q_{\alpha i} = -\hat{\kappa}_\alpha T_{\alpha,i}$ and the expansion

$$-\frac{\partial q_{\alpha i}}{\partial x_i} = \frac{\hat{\kappa}_\alpha}{T_\alpha}(\nabla T_\alpha)^2 - T_\alpha(q_{\alpha i}/T_\alpha)_{,i} \tag{94}$$

Eq. (93) can be written as

$$c_\alpha \frac{\partial s_\alpha}{\partial t} + c_\alpha u_{\alpha i} s_{\alpha,i} + (q_{\alpha i}/T_\alpha)_{,i} + \left(\frac{h_\alpha - \frac{|\boldsymbol{u}_\alpha|^2}{2}}{T_\alpha}\right)\left[\frac{\partial c_\alpha}{\partial t}\right]_{\text{col}} + \frac{u_{\alpha i}}{m_\alpha T_\alpha}\left[\frac{\partial p_{\alpha i}}{\partial t}\right]_{\text{col}} - \frac{1}{m_\alpha T_\alpha}\left[\frac{\partial w_\alpha}{\partial t}\right]_{\text{col}} = \frac{\hat{\kappa}_\alpha}{T_\alpha^2}(\nabla T_\alpha)^2 \tag{95}$$

For our intended purpose, Eq. (95) can be rewritten as

$$(c_\alpha s_\alpha)_{,t} + (c_\alpha u_{\alpha i} s_\alpha)_{,i} + (q_{\alpha i}/T_\alpha)_{,i} + \left(\frac{h_\alpha - \frac{|\boldsymbol{u}_\alpha|^2}{2}}{T_\alpha} - s_\alpha\right)\left[\frac{\partial c_\alpha}{\partial t}\right]_{\text{col}} + \frac{u_{\alpha i}}{m_\alpha T_\alpha}\left[\frac{\partial p_{\alpha i}}{\partial t}\right]_{\text{col}} - \frac{1}{m_\alpha T_\alpha}\left[\frac{\partial w_\alpha}{\partial t}\right]_{\text{col}} = \frac{\hat{\kappa}_\alpha}{T_\alpha^2}(\nabla T_\alpha)^2 \tag{96}$$

Observing that the quantity on the right-hand side of Eq. (96) is positive, an inequality of the following form can be obtained

$$(c_\alpha s_\alpha)_{,t} + (c_\alpha u_{\alpha i} s_\alpha)_{,i} + (q_{\alpha i}/T_\alpha)_{,i} + \left(\frac{h_\alpha - \frac{|\boldsymbol{u}_\alpha|^2}{2}}{T_\alpha} - s_\alpha\right)\left[\frac{\partial c_\alpha}{\partial t}\right]_{\text{col}} + \frac{u_{\alpha i}}{m_\alpha T_\alpha}\left[\frac{\partial p_{\alpha i}}{\partial t}\right]_{\text{col}} - \frac{1}{m_\alpha T_\alpha}\left[\frac{\partial w_\alpha}{\partial t}\right]_{\text{col}} \geq 0 \tag{97}$$

Eq. (97) is the statement for the production of entropy and serves as the basic stability condition for the hydrodynamic device equations.

REMARKS:

(i) Entropy production is governed by the Clausius–Duhem inequality. Clausius–Duhem inequality is also referred to as the second law of thermodynamics in some references (see [21] for a discussion). Thus, Eq. (97) is referred to as the local form of the Clausius–Duhem inequality for the conservation laws governing hydrodynamic semiconductor device equations.

(ii) Clausius–Duhem inequalities can be derived for problems governed by the conservation laws of mass, momentum and energy and have been derived for the Euler and Navier–Stokes equations [17].

(iii) It is important to note the contribution of collision terms to entropy production equation (97). Note also that the electric field terms do not contribute to entropy production.

(iv) The Clausius–Duhem inequality is also the physical stability condition for the conservation laws. Numerical formulations should not violate the Clausius–Duhem inequality.

Significance of entropy variables

The choice of variables employed to solve the set of conservation laws can play a significant role in the quality of numerical results. While any meaningful variables can be used to solve the conservation laws, we were motivated to use the entropy variables partially due to their success in producing superior results when applied to compressible Euler and Navier–Stokes equations [27]. Importantly, the use of entropy variables leads to a global statement of stability. A stability result is obtained by dotting the symmetrized system with $\boldsymbol{V}_\alpha$ (vector of entropy variables):

$$\boldsymbol{V}_\alpha \cdot (\tilde{\boldsymbol{A}}_{\alpha 0}\boldsymbol{V}_{\alpha,t} + \tilde{\boldsymbol{A}}_{\alpha i}\boldsymbol{V}_{\alpha,i} - (\tilde{\boldsymbol{K}}_{\alpha ij}\boldsymbol{V}_{\alpha,j})_{,i} - \boldsymbol{F}_\alpha) = 0 \tag{98}$$

Noting that (these results can be obtained directly from the definition of coefficient matrices obtained using the entropy variables)

$$\begin{aligned}
&\boldsymbol{V}_\alpha \cdot (\tilde{\boldsymbol{A}}_{\alpha i}\boldsymbol{V}_{\alpha,i}) = (\mathscr{H}_\alpha u_{\alpha i})_{,i} \\
&\boldsymbol{V}_\alpha \cdot \tilde{\boldsymbol{F}}^{\text{h}}_{\alpha,i} = \frac{q_{\alpha i}}{T_\alpha} \\
&\boldsymbol{V}_\alpha \cdot \boldsymbol{F}_\alpha = \frac{V_{\alpha 1}}{T_\alpha}\left[\frac{\partial c_\alpha}{\partial t}\right]_{\text{col}} + \frac{u_{\alpha i}}{m_\alpha T_\alpha}\left[\frac{\partial p_{\alpha i}}{\partial t}\right]_{\text{col}} - \frac{1}{m_\alpha T_\alpha}\left[\frac{\partial w_\alpha}{\partial t}\right]_{\text{col}}
\end{aligned} \tag{99}$$

Eq. (98) can be rewritten as

$$\mathscr{H}_{\alpha,t} + (\mathscr{H}_\alpha u_{\alpha i})_{,i} - (q_{\alpha i}/T_\alpha)_{,i} - V_{\alpha 1}\left[\frac{\partial c_\alpha}{\partial t}\right]_{\text{col}} - \frac{u_{\alpha i}}{m_\alpha T_\alpha}\left[\frac{\partial p_{\alpha i}}{\partial t}\right]_{\text{col}} + \frac{1}{m_\alpha T_\alpha}\left[\frac{\partial w_\alpha}{\partial t}\right]_{\text{col}} = -\nabla \boldsymbol{V}_\alpha \cdot \tilde{\boldsymbol{K}}_\alpha \nabla \boldsymbol{V}_\alpha \tag{100}$$

Substituting $\mathscr{H}_\alpha = -c_\alpha s_\alpha$ in Eq. (100), we obtain

$$(c_\alpha s_\alpha)_{,t} + (c_\alpha u_{\alpha i} s_\alpha)_{,i} + (q_{\alpha i}/T_\alpha)_{,i} + \left(\frac{h_\alpha - \frac{|u_\alpha|^2}{2}}{T_\alpha} - s_\alpha\right)\left[\frac{\partial c_\alpha}{\partial t}\right]_{\text{col}} + \frac{u_{\alpha i}}{m_\alpha T_\alpha}\left[\frac{\partial p_{\alpha i}}{\partial t}\right]_{\text{col}} - \frac{1}{m_\alpha T_\alpha}\left[\frac{\partial w_\alpha}{\partial t}\right]_{\text{col}} \geq 0 \tag{101}$$

Eq. (101) is identical to the Clausius–Duhem inequality, Eq. (97). That is, the Galerkin/least-squares finite element solution based on entropy variables automatically inherits the entropy production property of the hydrodynamic device equations.

Integrating Eq. (100) over Q obtains

$$\int_\Omega [\mathscr{H}_\alpha(T) - \mathscr{H}_\alpha(0)]\,d\Omega + \int_P \left[\mathscr{H}_\alpha u_{\alpha n} - \frac{q_{\alpha n}}{T_\alpha}\right] dP - \int_Q \left\{\frac{V_{\alpha 1}}{T_\alpha}\left[\frac{\partial c_\alpha}{\partial t}\right]_{\text{col}} + \frac{u_{\alpha i}}{m_\alpha T_\alpha}\left[\frac{\partial p_{\alpha i}}{\partial t}\right]_{\text{col}} - \frac{1}{m_\alpha T_\alpha}\left[\frac{\partial w_\alpha}{\partial t}\right]_{\text{col}}\right\} dQ = -\int_Q \nabla V_\alpha \cdot \tilde{\boldsymbol{K}}_\alpha \nabla V_\alpha \, dQ \tag{102}$$

Observing that the term on the right-hand side is non-positive, Eq. (102) can be expressed in an inequality form as

$$\int_\Omega [\mathscr{H}_\alpha(T) - \mathscr{H}_\alpha(0)]\,d\Omega + \int_P \left[\mathscr{H}_\alpha u_{\alpha n} - \frac{q_{\alpha n}}{T_\alpha}\right] dP - \int_Q \left\{\frac{V_{\alpha 1}}{T_\alpha}\left[\frac{\partial c_\alpha}{\partial t}\right]_{\text{col}} + \frac{u_{\alpha i}}{m_\alpha T_\alpha}\left[\frac{\partial p_{\alpha i}}{\partial t}\right]_{\text{col}} - \frac{1}{m_\alpha T_\alpha}\left[\frac{\partial w_\alpha}{\partial t}\right]_{\text{col}}\right\} dQ \leq 0 \tag{103}$$

Stability result from Galerkin/least-squares variation form

In this section it will be shown that the numerical algorithms discussed in this paper obey the Clausius–Duhem inequality and hence are stable formulations. Consider the statement of the finite element space–time weighted residual formulation given in Eq. (63).

Substituting $\boldsymbol{V}_\alpha^h$ for $\boldsymbol{W}_\alpha^h$ in Eq. (63) and summing over all the time slabs, i.e.

$$\sum_{n=0}^{N-1} (\boldsymbol{B}_{\text{GLS}}(\boldsymbol{V}^h, \boldsymbol{V}^h)_{\alpha n} - \boldsymbol{L}_{\text{GLS}}(\boldsymbol{V}^h)_{\alpha n}) = 0 \tag{104}$$

$$\sum_{n=0}^{N-1} \int_{Q_n} [-\boldsymbol{V}_{\alpha,t}^h \cdot \boldsymbol{U}_\alpha(\boldsymbol{V}_\alpha^h) - \boldsymbol{V}_{\alpha,i}^h \cdot \boldsymbol{F}_{\alpha i}^{\text{c}}(\boldsymbol{V}_\alpha^h) + \boldsymbol{V}_{\alpha,i}^h \cdot \tilde{\boldsymbol{K}}_{\alpha ij}(\boldsymbol{V}_\alpha^h)\boldsymbol{V}_{\alpha,j}^h - \boldsymbol{V}_\alpha^h \cdot \boldsymbol{F}_\alpha(\boldsymbol{V}_\alpha^h)]\,dQ + \sum_{n=0}^{N-1} \int_\Omega [\boldsymbol{V}_\alpha^h(t_{n+1}^-) \cdot \boldsymbol{U}_\alpha(\boldsymbol{V}_\alpha^h(t_{n+1}^-)) - \boldsymbol{V}_\alpha^h(t_n^+) \cdot \boldsymbol{U}_\alpha(\boldsymbol{V}_\alpha^h(t_{t_n}^-))]\,d\Omega + \sum_{n=0}^{N-1} \int_{P_n} [\boldsymbol{V}_\alpha^h \cdot (\boldsymbol{F}_{\alpha i}^{\text{c}}(\boldsymbol{V}_\alpha^h) - \boldsymbol{F}_{\alpha i}^{\text{h}}(\boldsymbol{V}_\alpha^h))n_i]\,dP + \sum_{n=0}^{N-1} \int_{Q_n^{\text{e}}} \mathscr{L}_\alpha \boldsymbol{W}_\alpha^h \cdot \tau_{\text{GLS}\alpha} \mathscr{L}_\alpha \boldsymbol{V}_\alpha^h \, dQ = 0 \tag{105}$$

Furthermore, note that

$$-\int_{Q_n} \boldsymbol{V}_{\alpha,i}^h \cdot \boldsymbol{F}_{\alpha i}^{\text{c}}(\boldsymbol{V}_\alpha^h)\,dQ = -\int_{P_n} \boldsymbol{V}_\alpha^h \boldsymbol{F}_{\alpha i}^{\text{c}} n_i \,dP + \int_{Q_n} \boldsymbol{V}_\alpha^h \boldsymbol{F}_{\alpha i,i}^{\text{c}}\,dQ$$

$$\int_{Q_n} -\boldsymbol{V}_{\alpha,t}^h \cdot \boldsymbol{U}_\alpha(\boldsymbol{V}_\alpha^h)\,dQ = \int_{Q_n} \boldsymbol{V}_\alpha^h \cdot \boldsymbol{U}_{\alpha,t}(\boldsymbol{V}_\alpha^h)\,dQ - \int_\Omega [\boldsymbol{V}_\alpha^h(t_{n+1}^-) \cdot \boldsymbol{U}_\alpha^h(t_{n+1}^-) - \boldsymbol{V}_\alpha^h(t_n^+) \cdot \boldsymbol{U}_\alpha^h(t_n^+)]\,d\Omega \tag{106}$$

Using Eqs. (99) and (106), Eq. (105) can be rewritten as

$$\sum_{n=0}^{N-1}\int_{Q_n}[-\mathscr{H}^h_{\alpha,t}-(\mathscr{H}^h_\alpha u^h_{\alpha i})_{,i}+\nabla V^h_\alpha\cdot\tilde{\boldsymbol{K}}_{\alpha ij}(V^h_\alpha)\nabla V^h_\alpha]\,dQ$$
$$-\sum_{n=0}^{N-1}\int_{Q_n}\left\{\frac{V^h_{\alpha 1}}{T^h_\alpha}\left[\frac{\partial c_\alpha}{\partial t}\right]_{\text{col}}+\frac{u^h_{\alpha i}}{m_\alpha T^h_\alpha}\left[\frac{\partial p_{\alpha i}}{\partial t}\right]_{\text{col}}-\frac{1}{m_\alpha T^h_\alpha}\left[\frac{\partial w_\alpha}{\partial t}\right]_{\text{col}}\right\}dQ$$
$$+\sum_{n=0}^{N-1}\int_\Omega[V^h_\alpha(t_n^+)\cdot(U^h_\alpha(t_n^+)-U^h_\alpha(t_n^-))]\,d\Omega-\sum_{n=0}^{N-1}\int_{P_n}\frac{q^h_{\alpha n}}{T^h_\alpha}\,dP+\sum_{n=0}^{N-1}\int_{Q_n^e}\mathscr{L}_\alpha W^h_\alpha\cdot\tau_{\text{GLS}\alpha}\mathscr{L}_\alpha V^h_\alpha\,dQ=0 \tag{107}$$

where $\mathscr{H}^h_\alpha=\mathscr{H}_\alpha(U_\alpha(V^h_\alpha))$, $T^h_\alpha=T_\alpha(V^h_\alpha)$, $q^h_{\alpha n}=q_{\alpha i}(V^h_\alpha)n_i$ and $u^h_{\alpha i}=u_{\alpha i}(V^h)$. Defining

$$\|s\|^2_Q=\int_Q s\,dQ \tag{108}$$

$$a_{\alpha n}=\int_\Omega V^h_\alpha(t_n^+)[[U_\alpha(V^h_\alpha(t_n))]]\,d\Omega-\int_\Omega(\mathscr{H}^h_\alpha(t_n^+)-\mathscr{H}^h_\alpha(t_n^-))\,d\Omega \tag{109}$$

and noting that

$$\int_Q\mathscr{H}^h_{\alpha,t}\,dQ=\int_\Omega[\mathscr{H}^h_\alpha(T^-)-\mathscr{H}^h_\alpha(0^+)]\,d\Omega-\sum_{n=1}^{N-1}\int_\Omega[\mathscr{H}^h_\alpha(t_n^+)-\mathscr{H}^h_\alpha(t_n^-)]\,d\Omega \tag{110}$$

Eq. (107) becomes

$$\int_\Omega[\mathscr{H}^h_\alpha(T^-)-\mathscr{H}^h_\alpha(0^+)]\,d\Omega+\int_P\left(\mathscr{H}^h_\alpha u^h_{\alpha n}-\frac{q^h_{\alpha n}}{T^h_\alpha}\right)dp$$
$$-\int_Q\left\{\frac{V^h_{\alpha 1}}{T^h_\alpha}\left[\frac{\partial c_\alpha}{\partial t}\right]_{\text{col}}+\frac{u^h_{\alpha i}}{m_\alpha T^h_\alpha}\left[\frac{\partial p_{\alpha i}}{\partial t}\right]_{\text{col}}-\frac{1}{m_\alpha T^h_\alpha}\left[\frac{\partial w_\alpha}{\partial t}\right]_{\text{col}}\right\}dQ$$
$$=-\|\tilde{\boldsymbol{K}}^{0.5}_\alpha\nabla V^h_\alpha\|^2_Q-\|\tau^{0.5}_{\text{GLS}\alpha}\mathscr{L}_\alpha V^h_\alpha\|^2_{\tilde{Q}}-\sum_{n=0}^{N-1}\alpha_{\alpha n} \tag{111}$$

In Eq. (111), all the quantities on the right-hand side are negative (see Appendix for the proof that $\alpha_{\alpha n}$ is positive). Therefore, Eq. (111) can be rewritten as

$$\int_\Omega[\mathscr{H}^h_\alpha(T^-)-\mathscr{H}^h_\alpha(0^+)]\,d\Omega+\int_P\left(\mathscr{H}^h_\alpha u^h_{\alpha n}-\frac{q^h_{\alpha n}}{T^h_\alpha}\right)dP$$
$$-\int_Q\left\{\frac{V^h_{\alpha 1}}{T^h_\alpha}\left[\frac{\partial c_\alpha}{\partial t}\right]_{\text{col}}+\frac{u^h_{\alpha i}}{m_\alpha T^h_\alpha}\left[\frac{\partial p_{\alpha i}}{\partial t}\right]_{\text{col}}-\frac{1}{m_\alpha T^h_\alpha}\left[\frac{\partial w_\alpha}{\partial t}\right]_{\text{col}}\right\}dQ\leqslant 0 \tag{112}$$

Eq. (112) is the exact analog of the entropy production inequality derived earlier in Eq. (103). Hence we conclude that our numerical formulation conform with Clausius–Duhem inequality and are entropy stable. In Eq. (111), the second and third terms on the right-hand side are the contributions from the least-squares term and the discontinuous Galerkin term, respectively. In the presence of small diffusion (the first term on the right-hand side of Eq. (111)) the stability comes primarily from the least-squares and the discontinuous Galerkin terms.

6. Numerical scheme for Poisson equation

A standard Galerkin finite element formulation is implemented for the Poisson equation. Advanced numerical methods like the Galerkin/least-squares formulation are not needed for the Poisson equation as the Galerkin finite element method is known to be stable for equations of type (4). The Galerkin finite element formulation for the Poisson equation can be summarized as follows:

Let the variational functional spaces S_p (subscript p denotes Poisson equation) and ϑ_p both consist of continuous functions with square integrable first derivatives. The solution space S_p is the set of all such functions satisfying the essential boundary conditions. The weighting function space ϑ_p is made up of functions whose value is zero where essential boundary conditions are specified, i.e.

$$\{S_p = \psi | \psi \in H^1(\Omega),\ \psi = g_p \text{ on } \Gamma_g\} \tag{113}$$

$$\{\vartheta_p = \bar{\psi} | \bar{\psi} \in H^1(\Omega),\ \bar{\psi} = 0 \text{ on } \Gamma_g\} \tag{114}$$

where g_p are the prescribed essential boundary conditions applied on the boundary Γ_g. Consider the following notation for the definition of the weak and Galerkin forms

$$a_p(u, v)_\Omega = \int_\Omega u_{,i} \theta v_{,i}\, \mathrm{d}\Omega \tag{115}$$

$$(u, v)_{\Gamma_{h_i}} = \int_{\Gamma_{h_i}} uv\, \mathrm{d}\Gamma \tag{116}$$

Weak form

The weak form is stated as follows: Given θ, f and h_i, find $\psi \in S_p$ such that for all $\bar{\psi} \in \vartheta_p$

$$B_p(\bar{\psi}, \psi) = L_p(\bar{\psi}) \tag{117}$$

where

$$B_p(\bar{\psi}, \psi) = a_p(\bar{\psi}, \psi)_\Omega \tag{118}$$

$$L_p(\bar{\psi}) = (\bar{\psi}, f)_\Omega + (\bar{\psi}, \theta h_i)_{\Gamma_{h_i}} \tag{119}$$

Note that $h_i = \psi_{,i} n_i$ are the natural boundary conditions prescribed on boundary Γ_{h_i}, and $f = -\varepsilon(c_1 - c_2 - N_D^+ + N_A^-)$.

Galerkin form

Let S_p^h and ϑ_p^h be the finite-dimensional approximations to S_p and ϑ_p, respectively. The Galerkin formulation can be stated as follows: Given θ, f and h_i find $\psi^h \in S_p^h$ such that for all $\bar{\psi}^h \in \vartheta_p^h$

$$B_p(\bar{\psi}^h, \psi^h) = L_p(\bar{\psi}^h) \tag{120}$$

Using a standard finite element discretization [14], a matrix form is obtained which is solved for the electrostatic potential ψ^h at all finite element nodes. The electric fields are computed at the center of each element and then projected onto the mesh nodes using smoothing procedures of a least-squares type [20].

6.1. Consistency

The consistency of Eq. (117) with the strong form of the boundary value problem may be verified as follows

$$\begin{aligned}
&B_p(\bar{\psi}, \psi) - L_p(\psi) = 0 \\
&\Rightarrow a_p(\bar{\psi}, \psi) - (\bar{\psi}, f)_\Omega - (\bar{\psi}, \theta h_i)_{\Gamma_{h_i}} = 0 \\
&\Rightarrow (\nabla\bar{\psi}, \theta\nabla\psi) - (\bar{\psi}, f)_\Omega - (\bar{\psi}, \theta h_i)_{\Gamma_{h_i}} = 0 \\
&\Rightarrow (\bar{\psi}, \theta\nabla\psi)_{\Gamma_{h_i}} - (\bar{\psi}, \nabla(\theta\nabla\psi))_\Omega - (\bar{\psi}, f)_\Omega - (\bar{\psi}, \theta h_i)_{\Gamma_{h_i}} = 0 \\
&\Rightarrow -(\bar{\psi}, (\nabla(\theta\nabla\psi) + f))_\Omega + (\bar{\psi}, \theta(\nabla\psi - h_i))_{\Gamma_{h_i}} = 0
\end{aligned} \tag{121}$$

The above equation gives

$$\nabla(\theta \nabla\psi) + f = 0 \quad \text{on } \Omega \tag{122}$$

which is the original equation (Eq. (4)) to be solved and

$$\nabla\psi n_i = h_i \quad \text{on } \Gamma_{h_i} \tag{123}$$

which are the prescribed natural boundary conditions. Hence, the consistency to the original form of the equation to be solved is verified.

6.2. Stability

Stability is established as follows

$$B_p(\bar{\psi}, \bar{\psi}) = a_p(\bar{\psi}, \bar{\psi}) = \theta \|\nabla\bar{\psi}\|_\Omega^2 \tag{124}$$

Eq. (124) means that the left-hand side matrix operator is positive definite, which is basically the stability statement for the Galerkin finite element formulation [16].

7. Solution schemes

The coupled Poisson and the two-carrier hydrodynamic equations are solved employing a staggered scheme, which resembles the popular Gummel procedure [10] (Fig. 1). The Poisson equation is first solved for the electrostatic potential. The electric fields are computed from the obtained potential by using smoothing procedures of a least-squares type. The computed electric field values are then used to solve the electron hydrodynamic equations for electron concentration, velocities and temperature. The electron hydrodynamic equations also require the hole concentration and since the hole concentration at the current iteration is not available, the value from the previous iterate is used. We next solve the hole hydrodynamic equations for hole concentration, velocities and temperature. Since the hole hydrodynamic equations are coupled to the electron concentration, either the currently computed electron concentration or the one computed in the previous iteration can be used. A faster convergence can be obtained if the currently available electron concentration is used. The computed concentrations for electrons and holes provide a new source term to the Poisson equation. This procedure of

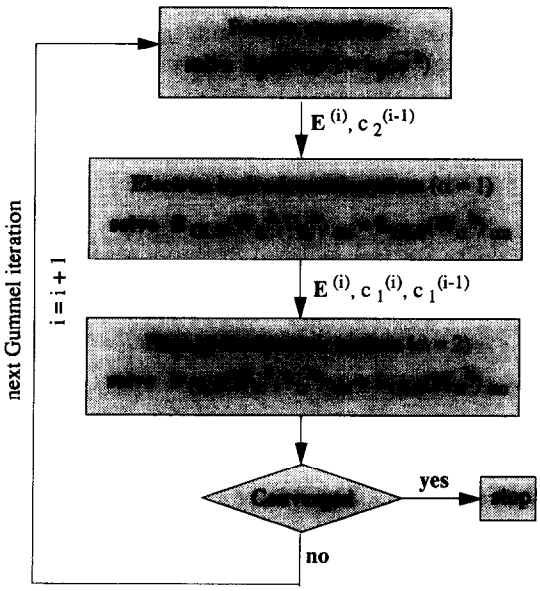

Fig. 1. A staggered scheme for solving coupled two-carrier hydrodynamic device equations.

alternatively solving the Poisson and the electron and hole hydrodynamic equations is repeated until all the equations are solved to a desired tolerance.

A number of advantages can be accounted for the proposed staggered scheme. First, it is simple and the storage requirement is much less than treating the coupled system as a whole. Second, the method converges for almost all arbitrary initial guesses. Third, the separation of the two systems allows the use of efficient solvers developed for each system. For instance, a non-symmetric equation solver is needed for the electron and hole hydrodynamic systems but only a symmetric solver is needed for the Poisson equation. For some problems, we can also minimize the cost by solving the Poisson equation as accurate as possible but relaxing the tolerance for the solution of the hydrodynamic system during the iterative process. The fourth advantage is that we can study the error estimators for each system separately, thus simplifying the complexity of the problem. However, by solving all the equations as a single system, a much faster convergence to steady-state solution can be obtained, if good initial guesses can be provided.

8. Numerical examples

In this section, numerical examples are presented to demonstrate the performance of the finite element method described in the previous sections. Examples of one- and two-dimensional two-carrier pn diodes are solved in forward bias. The operation of pn diodes poses several challenges to the numerical schemes as the examples involve localized regions (also termed as depletion regions) where the carrier concentrations vary over several orders of magnitude within a distance of few tenths of a micron. By presenting numerical results for these examples a number of issues are demonstrated: First, the single-carrier formulation can be extended to two-carriers in a straight forward manner. Second the performance of the numerical scheme (stability, robustness and accuracy) are not effected by the addition of a second carrier or the device operation in high level injection and finally, the proposed formulation requires minimal changes to extend the computer program for single carrier simulation to incorporate the second carrier.

8.1. Example 1

The first example is a one-dimensional silicon n^+p diode which is 1.0 μm in length and is operated in forward bias. The n^+-region is doped with $1.0 \times 10^{18}/\text{cm}^3$ and the p-region is doped with $1.0 \times 10^{16}/\text{cm}^3$. The n^+ region is 0.2 μm is length and the doping in the n^+p transition region varies as a Gaussian function with $\sigma = 0.01$ μm. The geometry of the diode is shown in Fig. 2. The boundary conditions applied are given as follows:

At $x = 0$ μm $\quad c_1 = 9.9 \times 10^{17}\ \text{cm}^{-3}$
$T_1 = T_2 = 300$ K and
$\psi = \psi_\beta(N_D)$

At $x = 1.0$ μm $\quad c_2 = 1.0 \times 10^{16}\ \text{cm}^{-3}$
$T_1 = T_2 = 300$ K and
$\psi = -\psi_\beta(N_A) + \psi_{\text{appl}}$

where $\psi_b(N)$ is the built-in potential (a function of doping, N) defined as

$$\psi_b(N) = \frac{k_b T_0}{\varepsilon} \ln\left(\frac{N}{c_{\text{int}}}\right)$$

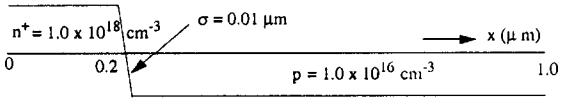

Fig. 2. Geometry of a one-dimensional pn diode.

and N_D, N_A are the net donor and acceptor concentrations. ψ_{appl} denotes the applied bias which is taken as 1.0 V. The initial conditions for the time-marching scheme that we employ to reach steady state are as follows:

$$\text{At } t = 0 \quad c_1(x,0) = \frac{N_D - N_A}{2} + \left[\left(\frac{N_D - N_A}{2}\right)^2 + c_{int}^2\right]^{0.5}; \qquad c_2(x,0) = \frac{c_{int}^2}{c_1(x,0)}$$

$$u_1(x,0) = u_2(x,0) = 0.0; \quad \text{and}$$

$$T_1(x,0) = T_2(x,0) = T_0$$

In this problem a continuation method is used, i.e. a bias increment of 0.2 V is applied starting at 0 V. We used 1001 mesh points with a uniform mesh spacing of 10 Å. A non-uniform mesh of 250 mesh points with finer spacing in the depletion region can also be used to obtain the same accuracy results as shown in this paper. We are currently designing adaptive algorithms to further investigate the issue of optimal meshes without affecting the accuracy of the solution. The steady-state results for this problem as shown in Figs. 3–10.

Figs. 3 and 4 show the electron and hole concentrations, respectively. The electron and hole concentrations vary by several orders of magnitude in a very small localized region. The electron concentration in the p-region and the hole concentration in the n-region increase significantly as the applied bias is increased. Figs. 5 and 6 show the electron and hole velocity, respectively. As the applied bias increases the electron velocity increases sharply and steeply near $X = 1$ μm. Also notice the steep drop in the hole velocity near $X = 1$ μm. These velocity components contribute to a significant increase

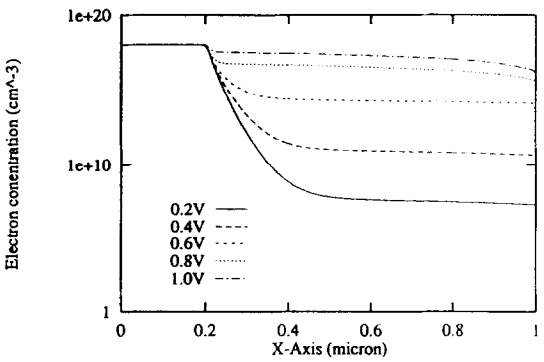

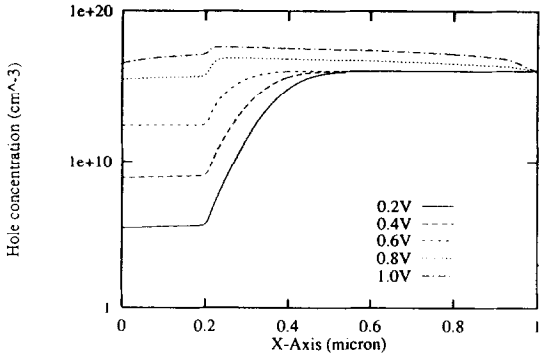

Fig. 3. Electron concentration (cm $^{-3}$) in steady state for forward biases of 0.2 V to 1.0 V with 0.2 V increments.

Fig. 4. Hole concentration (cm $^{-3}$) in steady state for forward biases of 0.2 V to 1.0 V with 0.2 V increments.

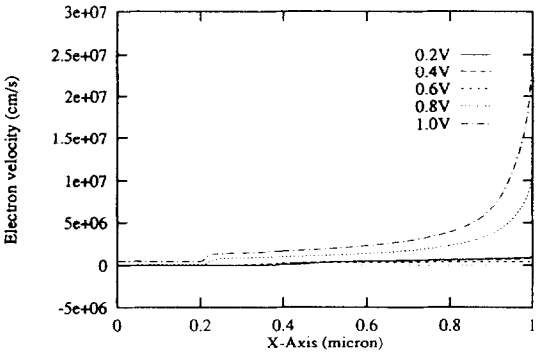

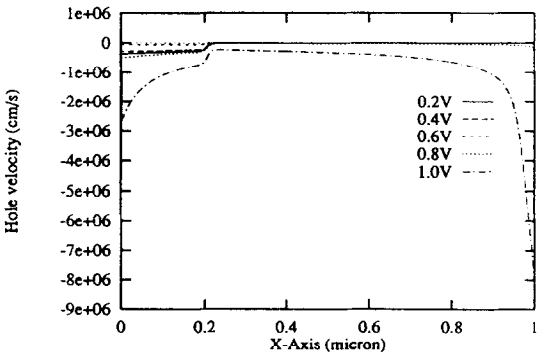

Fig. 5. Electron velocity (cm/s) in steady state for forward biases of 0.2 to 1.0 V with 0.2 V increments.

Fig. 6. Hole velocity (cm/s) in steady state for forward biases of 0.2 to 1.0 V with 0.2 V increments.

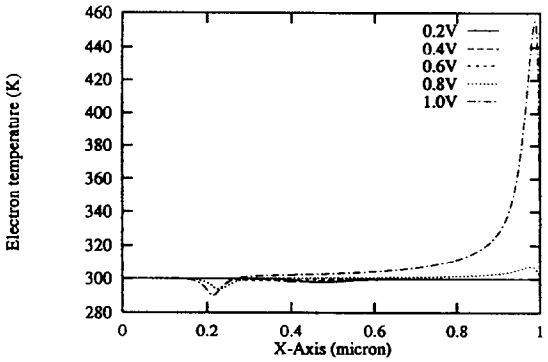

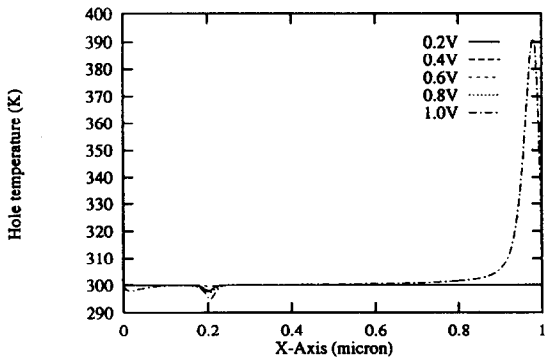

Fig. 7. Electron temperature (K) in steady state for forward biases of 0.2 V to 1.0 V with 0.2 V increments.

Fig. 8. Hole temperature (K) in steady state for forward biases of 0.2 V to 1.0 V with 0.2 V increments.

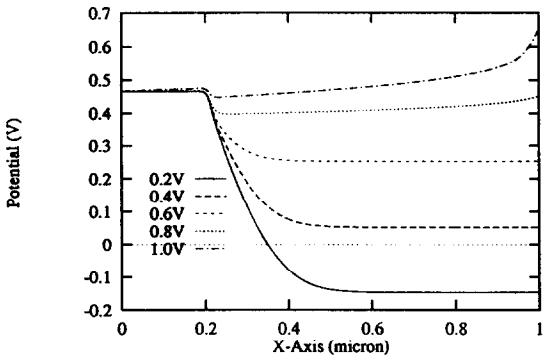

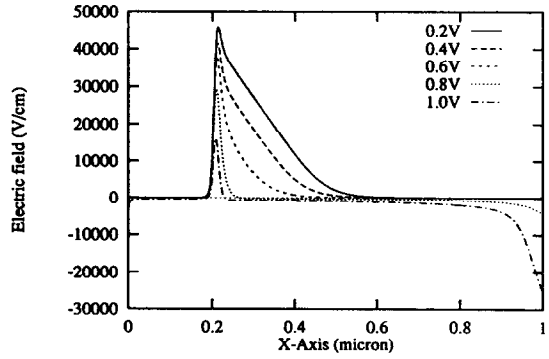

Fig. 9. Electrostatic potential (V) in steady state for forward biases of 0.2 V to 1.0 V with 0.2 V increments.

Fig. 10. Electric field (V/cm) in steady state for forward biases of 0.2 V to 1.0 V with 0.2 V increments.

in current as the applied bias is increased. Figs. 7 and 8 show the electron and hole temperature, respectively. The electron and hole temperatures undergo rapid changes near $X = 1$ μm for applied bias of 1.0 V. This is because of the operation of the diode in high level injection. For low applied biases, small temperature drops can be observed in the depletion region. Fig. 9 shows the variation of the electrostatic potential in the diode and Fig. 10 shows the variation of the electric field which is the negative gradient of potential.

8.2. Example 2

The second example is a two-dimensional silicon pn diode which is 3.5 μm × 2.5 μm. The n^+-region has a doping of $1.0 \times 10^{17}\,\mathrm{cm}^{-3}$ and the p-region has a doping of $1.0 \times 10^{15}\,\mathrm{cm}^{-3}$. The transition between the n^+ and p region is not abrupt and is treated as a Gaussian variation with $\sigma = 0.4$ μm. Two contacts are placed along the boundaries of the device and device is operated in forward bias. Both contacts are assumed to be ohmic. The geometry of the diode and the placement of the contacts are shown in Fig. 11.

The n contact extends up to a distance of 0.5 μm from the top left corner and the p contact covers the entire base. For forward bias operation of the diode, 0.0 V is applied on the n contact and 0.8 V is applied on the p contact. The boundary conditions are applied as follows:

(i) Along contact 1–2: $c_2 = 1.0 \times 10^{15}\,\mathrm{cm}^{-3}$, $u_2 = 0\,\mathrm{cm/s}$ and $\psi = -\psi_b(N_A) + 0.8$ V.

(ii) Along boundaries 2–3 and 1–5: $u_1 = u_2 = 0\,\mathrm{cm/s}$ and $\partial\psi/\partial n = 0$ (Neumann boundary condition for potential).

(iii) Along boundary 3–4: $v_1 = v_2 = 0\,\mathrm{cm/s}$ and $\partial\psi/\partial n = 0$.

(iv) Along contact 4–5: $c_1 = 1.0 \times 10^{17}\,\mathrm{cm}^{-3}$, $T_1 = T_0$ and $\psi_b(N_D)$.

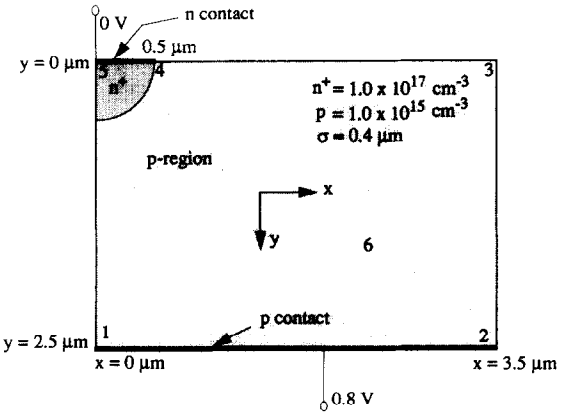

Fig. 11. Geometry of a two-dimensional pn diode.

Note that the boundary conditions specified above do not necessarily follow the boundary conditions discussed in Section 4.4. This is because 0.8 V can be considered as a high forward bias or a high level injection case and in this case $c_1 c_2 = c_{\text{int}}^2$ is not a reasonable approximation and hence the concentration for minority carriers is typically not known at outflow boundaries. Hence, in order to strictly impose the correct number of boundary conditions, mixed type of boundary conditions or their variants are needed and this can be quite challenging. Instead, we have imposed the boundary conditions in terms of the quantities that are generally known. This method of specification can lead to over specified or under specified systems of equations and robust numerical schemes are needed to guarantee convergence. Our results indicate that the numerical scheme proposed in this paper is not very sensitive to the specification of boundary conditions. However, the convergence of the algorithm could be slow. Adhering to the strict imposition of boundary conditions discussed in Section 4.4 can lead to boundary layers near the contacts. The reader should however note that the boundary conditions discussed in Section 4.4 are applied to low forward bias regime.

The initial conditions are given as follows:

$$\text{At } t = 0 \quad c_1(x, y, 0) = \frac{N_D - N_A}{2} + \left[\left(\frac{N_D - N_A}{2}\right)^2 + c_{\text{int}}^2\right]^{0.5}, \qquad c_2(x, y, 0) = \frac{c_{\text{int}}^2}{c_1(x, y, 0)}$$

$$u_1(x, y, 0) = u_2(x, y, 0) = 0.0$$

$$v_1(x, y, 0) = v_2(x, y, 0) = 0.0$$

$$T_1(x, y, 0) = T_2(x, y, 0) = T_0$$

For this problem a continuation method is used with a bias increment of 0.1 V starting from 0 V. A mesh of 64×47 nodes is employed. The steady-state results for this problem are shown in Figs. 12–22.

Figs. 12 and 13 show the electron and hole concentrations, respectively. Similar to the one-dimensional example the electron and hole concentrations vary over several orders of magnitude in small localized regions and the numerical algorithm proposed is able to resolve such a sharp gradient effectively. Figs. 14 and 15 show the electron and hole velocities in the x-direction, respectively. Velocity overshoot can be observed close to the termination of n-contact. The velocity overshoot could be the result of the discontinuity in the velocity boundary condition. This velocity overshoot phenomenon does not occur in low forward bias cases. Figs. 16 and 17 show the electron and hole velocities in the y-direction, respectively. The electron and hole temperatures shown in Figs. 18 and 19, respectively, indicate that the electrons get heated more than the holes. The hole temperatures are very close to the room temperatures while the electron temperatures are slightly higher in the p-region. Fig. 20 shows the electrostatic potential and Figs. 21 and 22 show the electric fields in the x and y directions, respectively.

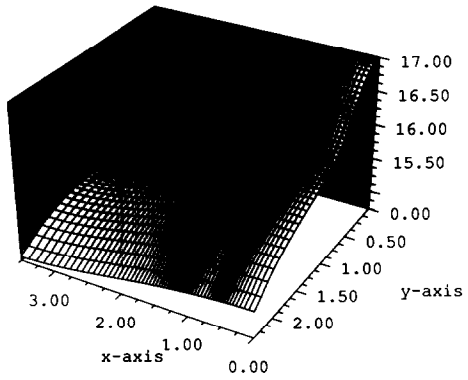

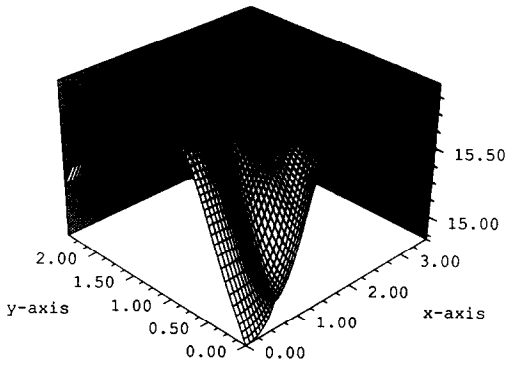

Fig. 12. Electron concentration (cm^{-3}) in steady state for 2D pn diode in forward bias of 0.8 V.

Fig. 13. Hole concentration (cm^{-3}) in steady state for 2D pn diode in forward bias of 0.8 V.

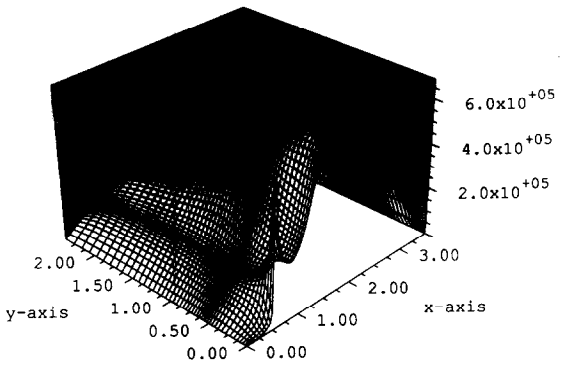

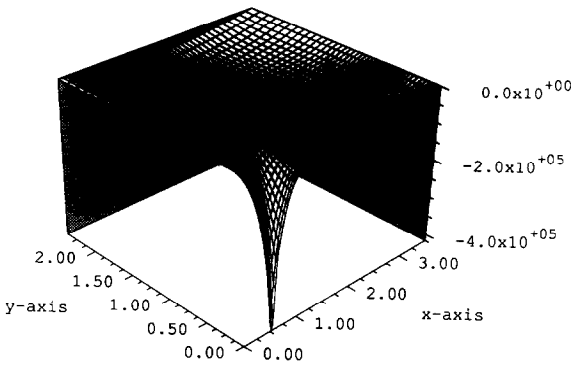

Fig. 14. Electron x-velocity (cm/s) in steady state for 2D pn diode in forward biases of 0.8 V.

Fig. 15. Hole x-velocity (cm/s) in steady state for 2D pn diode in forward biases of 0.8 V.

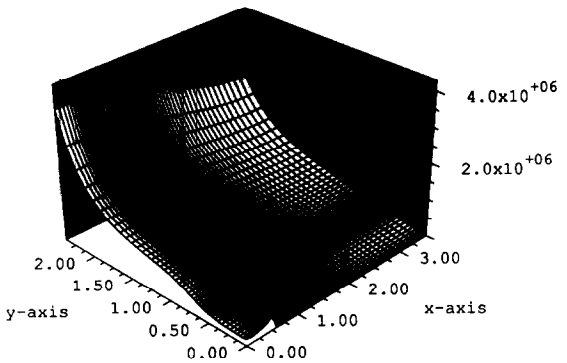

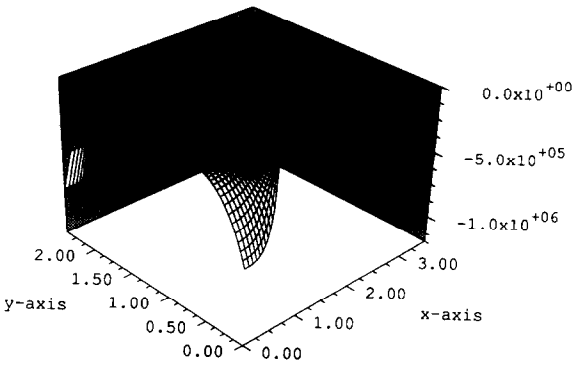

Fig. 16. Electron y-velocity (cm/s) in steady state for 2D pn diode in forward biases of 0.8 V.

Fig. 17. Hole y-velocity (cm/s) in steady state for 2D pn diode in forward biases of 0.8 V.

9. Conclusions

A space–time Galerkin/least-squares finite element method, proposed and implemented for two-carrier hydrodynamic equations, is able to solve the coupled semiconductor device equations efficiently and accurately. The proposed numerical algorithms are shown to be stable and consistent. A Clausius–

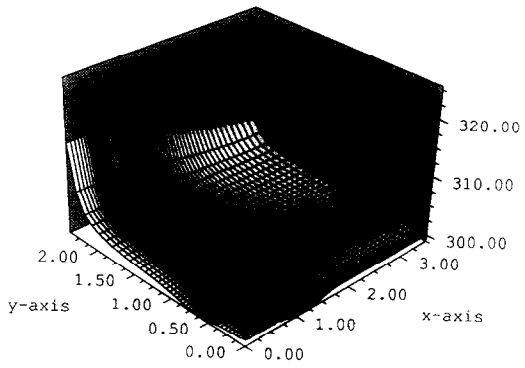

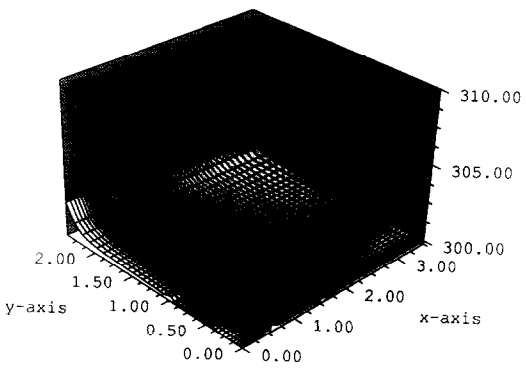

Fig. 18. Electron temperature (K) in steady state for 2D pn diode in forward biases of 0.8 V.

Fig. 19. Hole temperature (K) in steady state for 2D pn diode in forward biases of 0.8 V.

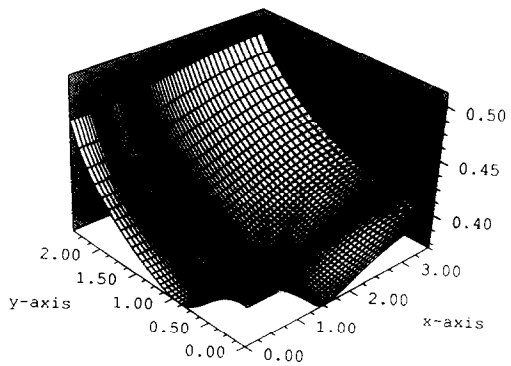

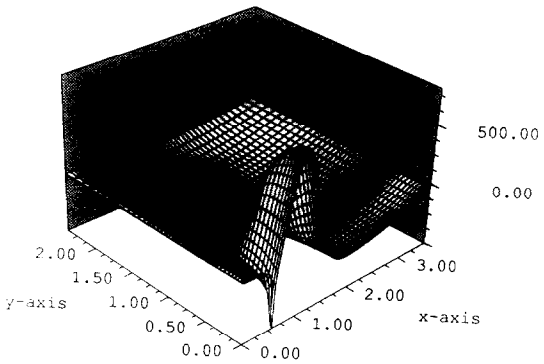

Fig. 20. Electrostatic potential (V) in steady state for 2D pn diode in forward biases of 0.8 V.

Fig. 21. X—Electric field (V/cm) in steady state for 2D pn diode in forward biases of 0.8 V.

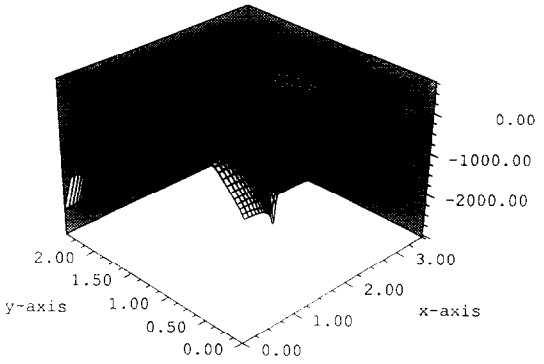

Fig. 22. Y—Electric field (V/cm) in steady state for 2D pn diode in forward biases of 0.8 V.

Duhem inequality is derived for the hydrodynamic conservation laws and the entropy variable based approach is shown to automatically satisfy this inequality.

Theoretical results for boundary conditions are derived for the well-posedness of the hydrodynamic model. The practical difficulty in imposing the theoretically observed results is addressed for high forward bias voltages. A bridge needs to be built between theory and practice for special cases and this is a topic for further investigation.

In earlier papers [1, 8, 9], it was observed that the heat conduction term plays a very important role that can significantly affect the accuracy of the solution. Hence, new models have been proposed in

which the coefficient of heat conductivity is reduced [11]. For the numerical examples shown in this paper, it was observed that the results are not significantly different with old and new heat conduction models.

The numerical scheme proposed in this paper is computationally very intensive. Several hours of computing time could be needed if the simulations were to be performed on workstations. Parallel algorithms have been developed and implemented to efficiently solve complex device examples on state-of-the-art parallel machines. A discussion of the parallel implementation on a MIMD distributed memory computer is beyond the scope of this paper. Our current and future efforts involve the design and development of adaptive, parallel adaptive algorithms and three-dimensional device simulation.

Acknowledgments

The authors would like to thank Prof. T.J.R. Hughes for helpful discussions on the finite element formulation for two-carrier devices and Drs. Ke-Chih Wu, Zhiping Yu and Edwin Kan for many helpful suggestions. This research is sponsored by ARPA through contract #DAAL 02-91-C-0043.

Appendix

LEMMA.

$$a_{\alpha n} = \int_{\Omega} \boldsymbol{V}^h(t_n^+)[[\boldsymbol{U}(\boldsymbol{V}^h(t_n))]]\,\mathrm{d}\Omega - \int_{\omega} (\mathscr{H}^h(t_n^+) - \mathscr{H}^h(t_n^-))\,\mathrm{d}\Omega \geqslant 0$$

PROOF. Using Taylor's formula with integral form of remainder

$$\begin{aligned}
&\mathscr{H}^h(t_n^-) - \mathscr{H}^h(t_n^+) + \boldsymbol{V}^h(t_n^+)[[\boldsymbol{U}(\boldsymbol{V}^h(t_n))]] \\
&\quad = \int_0^1 (1-\varepsilon)[[\boldsymbol{U}(\boldsymbol{V}^h(t_n))]] \cdot \tilde{\boldsymbol{A}}_0^{-1}(\boldsymbol{U}(t_n^+) - \varepsilon[[\boldsymbol{U}(t_n)]])[[\boldsymbol{U}(t_n)]]\,\mathrm{d}\varepsilon \\
&\quad \geqslant \hat{c}|[[\boldsymbol{U}(t_n)]]|^2_{\tilde{A}_0^{-1}}
\end{aligned}$$

where $|X|^2_{\tilde{A}_0^{-1}} = X \cdot \tilde{A}_0^{-1} X$

Therefore,

$$a_{\alpha n} = \int_{\Omega} \boldsymbol{V}^h(t_n^+)[[\boldsymbol{U}(\boldsymbol{V}^h(t_n))]]\,\mathrm{d}\Omega - \int_{\Omega} (\mathscr{H}^h(t_n^+) - \mathscr{H}^h(t_n^-))\,\mathrm{d}\Omega \geqslant 0$$

References

[1] N.R. Aluru, A. Raefsky, P.M. Pinsky, K.H. Law, R.J.G. Goossens and R.W. Dutton, A finite element formulation for the hydrodynamic semiconductor device equations, Comput. Methods Appl. Mech. Engrg. 107 (1993) 269–298.

[2] N.R. Aluru, K.H. Law, P.M. Pinsky, A. Raefsky, R.J.G. Goossens and R.W. Dutton, Space–time Galerkin/least-squares finite element formulation for the hydrodynamic device equations, IEICE Trans. Electron E77-C(2) (1994) 227–235.

[3] N.R. Aluru and K.H. Law, A study on the well-posed boundary conditions for the full hydrodynamic model of semiconductor devices, Technical Report—October 1993, Integrated Circuits Laboratory, Stanford University, Stanford, CA.

[4] G. Baccarani and M.R. Wordeman, An investigation of steady-state velocity overshoot in silicon, Solid-State Electron. 28 (1985) 407–416.

[5] K. Blotekjaer, Transport equations for electrons in two-valley semiconductors, IEEE Trans. Electron. Dev. ED-17 (1970) 38–47.

[6] S.W. Bova and G.F. Carey, An analysis of the time-dependent hydrodynamic device equations, Proc. Intl. Workshop Comp. Elec., Univ. of Illinois, pp. 91–94, 28–29 May 1992.

[7] D. Chen, E.C. Kan, U. Ravaioli, Z. Yu and R.W. Dutton, A self-consistent discretization scheme for current and energy transport equations, presented at IV Int. Conf. on Simulation of Semiconductor Devices and Processes (SISDEP), Zurich, 12–14 Sep. 1991.
[8] E. Fatemi, J.W. Jerome and S. Osher, Solution of the hydrodynamic device model using high-order nonoscillatory shock capturing algorithms, IEEE Trans. CAD 10 (1991) 232–244.
[9] C.L. Gardner, J.W. Jerome and D.J. Rose, Numerical methods for the hydrodynamic device model: subsonic flow, IEEE Trans. CAD 8 (1989) 501–507.
[10] K.K. Gummel, A self-consistent iterative scheme for one-dimensional steady state transistor calculations, IEEE Trans. Electron. Dev. ED-11 (1964) 455–465.
[11] A. Gnudi, F. Odeh and M. Rudan, Investigation of non-local transport phenomena in small semiconductor devices, European Trans. Telecomm. 1 (1990) 307–313.
[12] B. Gustafson and A. Sundstrom, Incompletely parabolic problems in fluid dynamics, SIAM J. Appl. Math. 35 (1978) 343–357.
[13] A. Harten, On the symmetric form of the systems of conservation laws with entropy, J. Comp. Phys. 49 (1983) 151–164.
[14] T.J.R. Hughes, The finite element method: Linear Static and Dynamic Finite Element Analysis (Prentice-Hall, Englewood Cliffs, NJ, 1987).
[15] T.J.R. Hughes and A. Brooks, A theoretical framework for Petrov–Galerkin methods with discontinuous weighting functions. Application to the streamline upwind procedure, in: Gallagher et al., eds., Finite Elements in Fluids, Vol. 4 (1982) 47–65.
[16] T.J.R. Hughes, L.P. Franca and G.M. Hulbert, A new finite element formulation for computational fluid dynamics: VIII. The Galerkin/least-squares method for advective–diffusive systems, Comput. Methods Appl. Mech. Engrg. 58 (1986) 173–189.
[17] T.J.R. Hughes, L.P. Franca and M. Mallet, A new finite element formulation for computational fluid dynamics: I. Symmetric forms of the compressible and Euler and Navier–Stokes equations and the second law of thermodynamics, Comput. Methods Appl. Mech. Engrg. 54 (1986) 223–234.
[18] T.J.R. Hughes and M. Mallet, A new finite element formulation for computational fluid dynamics: III. The generalized streamline operator for multidimensional advective–diffusive systems, Comput. Methods Appl. Mech. Engrg. 58 (1986) 305–328.
[19] C. Johnson, U. Navert and J. Pitkaranta, Finite element methods for linear hyperbolic problems, Comput. Methods Appl. Mech. Engrg. 45 (1984) 285–312.
[20] R.L. Lee, P.M. Gresho and R.L. Sani, Smoothing techniques for certain primitive variable solutions of the Navier–Stokes equations, Int. J. Numer. Methods Engrg. 14 (1979) 1785–1804.
[21] J.E. Marsden and T.J.R. Hughes, Mathematical Foundations of Elasticity (Prentice-Hall, Englewood Cliffs, NJ, 1983).
[22] J. Oliger and A. Sundstrom, Theoretical and practical aspects of some initial boundary value problems in fluid dynamics, SIAM J. Appl. Math., 35 (1978) 419–446.
[23] M.R. Pinto, Comprehensive semiconductor device simulation for silicon ULSI, Dept. of Elec. Engrg., Ph.D. Thesis, Stanford University, Aug. 1990.
[24] M. Rudan, F. Odeh and J. White, Numerical solution of the hydrodynamic model for a one-dimensional device, COMPEL 6 (1987) 151–170.
[25] S. Selberherr, An Analysis and Simulation of Semiconductor Devices (New York: Springer-Verlag, 1984).
[26] F. Shakib, Finite element analysis of the compressible Euler and Navier–Stokes equations, Dept. of Mech. Engrg., Ph.D. Thesis, Stanford University, Nov. 1988.
[27] F. Shakib, T.J.R. Hughes and Z. Johan, A new finite element formulation for computational fluid dynamics: X. The compressible Euler and Navier–Stokes equations, Comput. Methods Appl. Mech. Engrg. 89 (1991) 141–219.
[28] M. Sharma and G.F. Carey, Semiconductor device modeling using flux upwind finite elements, COMPEL 8 (1989) 219–224.
[29] J. Strikwerda, Initial boundary value problems for incompletely parabolic systems, Ph.D. Thesis, Dept. of Math., Stanford Univ., Stanford, CA, 1976.
[30] E. Thomann and F. Odeh, On the well-posedness of the two-dimensional hydrodynamic model for semiconductor devices, COMPEL 9 (1990) 45–57.